

Translocator protein is a marker of activated microglia in rodent models but not human neurodegenerative diseases

Erik Nutma

Amsterdam UMC - Location VUmc <https://orcid.org/0000-0002-7332-1636>

Nurun Fancy

Imperial College London

Manuel Marzin

Amsterdam UMC

Stergios Tsartsalis

Imperial College

Robert C.J Muirhead

Imperial College London

Irene Falk

NIH

Joy de Bruin

Amsterdam UMC - Location VUmc

David Hollaus

Amsterdam UMC - Location VUmc

Robin Pieterman

Amsterdam UMC - Location VUmc

Jasper Anink

Amsterdam UMC - Location AMC

David Story

Siddharthan Chandran

University of Edinburgh

Jiabin Tang

Imperial College

Maria Trolese

Mario Negri Institute for Pharmacological Research IRCCS <https://orcid.org/0000-0003-4471-2491>

Takashi Saito

Nagoya City University <https://orcid.org/0000-0002-9659-9251>

Takaomi Saido

RIKEN Brain Science Institute

Maria Weinert

Imperial College London <https://orcid.org/0000-0001-6187-1000>

Craig Moore

<https://orcid.org/0000-0003-3333-435X>

Caterina Bendotti

Istituto di Ricerche Farmacologiche Mario Negri, Milan (Italy)

Eleonora Aronica

University of Amsterdam

Carola Radulescu

Imperial College London

Steve Jacobson

NINDS/NIH

Samuel Barnes

Imperial College London <https://orcid.org/0000-0003-4030-6453>

David Hampton

University of Edinburgh

Paul van der Valk

Amsterdam UMC - Location VUmc

Paul Matthews

Imperial College London <https://orcid.org/0000-0002-1619-8328>

Sandra Amor

Department of Pathology, Amsterdam UMC/Centre for Neuroscience and Trauma, Blizard Institute, Barts and the London School of Medicine & Dentistry, Queen Mary University of London

David Owen (✉ d.owen@imperial.ac.uk)

Imperial College London <https://orcid.org/0000-0002-1198-7563>

Article

Keywords: ALS, AD, MS, TSPO, microglia

Posted Date: March 23rd, 2022

DOI: <https://doi.org/10.21203/rs.3.rs-1420033/v1>

License:   This work is licensed under a Creative Commons Attribution 4.0 International License.

[Read Full License](#)

1 **Translocator protein is a marker of activated microglia in rodent** 2 **models but not human neurodegenerative diseases**

3 Erik Nutma^{1,†}, Nurun Fancy^{2,3,†}, Manuel C. Marzin¹, Stergios Tsartsalis^{2,3,4}, Robert C.J.
4 Muirhead^{2,3}, Irene Falk^{5,6}, Joy de Bruin¹, David Hollaus¹, Robin Pieterman¹, Jasper Anink⁷,
5 David Story⁸, Siddharthan Chandran⁸, Jiabin Tang^{2,3}, Maria C. Trolese⁹, Takashi Saito¹⁰,
6 Takaomi C. Saido¹¹, Maria Weinert², Craig S. Moore¹², Caterina Bendotti⁹, Eleonora
7 Aronica⁷, Carola I. Radulescu^{2,3}, Samuel J. Barnes^{2,3}, David W. Hampton⁸, Paul van der
8 Valk¹, Steven Jacobson⁵, Paul M. Matthews^{2,3}, Sandra Amor^{1,13,*}, David R. Owen^{2,*}

9 ¹Department of Pathology, Amsterdam UMC – Location VUmc, Amsterdam, the Netherlands

10 ²Department of Brain Sciences, Imperial College London, UK

11 ³UK Dementia Research Institute at Imperial College London, UK

12 ⁴Department of Psychiatry, University of Geneva, Switzerland

13 ⁵Viral Immunology Section, NIH, Bethesda, Maryland, USA

14 ⁶Flow and Imaging Cytometry Core Facility, NIH, Bethesda, Maryland, USA

15 ⁷Department of Pathology, Amsterdam UMC – Location AMC, Amsterdam, the Netherlands

16 ⁸Centre for Clinical Brain Sciences, The University of Edinburgh, Edinburgh, United Kingdom

17 ⁹Department of Neuroscience, Mario Negri Institute for Pharmacological Research IRCCS, Milan, Italy

18 ¹⁰Laboratory for Proteolytic Neuroscience, RIKEN Brain Science Institute, Wako-shi, Saitama, Japan

19 ¹¹Department of Neurocognitive Science, Institute of Brain Science, Nagoya City University, Japan

20 ¹²Division of Biomedical Sciences, Memorial University of Newfoundland, Canada

21 ¹³Department of Neuroscience and Trauma, Blizard Institute, Barts and the London School of Medicine &
22 Dentistry, Queen Mary University of London, London, UK

23 [†] shared first authorship

24 ^{*}shared senior authorship

25 **Running title:** TSPO expression in neurodegenerative diseases

26 Addresses of corresponding authors:

27 Professor Sandra Amor

28 Department of Pathology

29 Amsterdam UMC, location VUmc

30 1081 HV Amsterdam, the Netherlands

31 s.amor@amsterdamumc.nl

32 Tel: +31 20 44 42 898

33 And

34 Dr. David Owen

35 Department of Brain Sciences

36 Du Cane Road

37 Hammersmith Hospital

38 Imperial College London

39 London W12 0HS

40 d.owen@imperial.ac.uk

41 Tel: +44 203 313 6195

42 **Abstract**

43 Microglial activation plays central roles in neuro-inflammatory and neurodegenerative
44 diseases. Positron emission tomography (PET) targeting 18kDa Translocator Protein
45 (TSPO) is widely used for localising inflammation *in vivo*, but its quantitative
46 interpretation remains uncertain. For the first time, we show that TSPO gene and protein
47 expression increases in activated microglia in mouse brain disease models postmortem,
48 but does not change in a non-human primate (*Callithrix jacchus*) disease model or in
49 common neurodegenerative and neuroinflammatory human diseases. We describe
50 genetic divergence in the TSPO gene promoter that may be responsible for this, which is
51 consistent with the hypothesis that the increase in TSPO in activated myeloid cells is
52 unique to a subset of species within the *Muroidea* superfamily of rodents. These data
53 emphasise that TSPO expression in human myeloid cells is related to different
54 phenomena than in mice, and that TSPO PET reflects density of inflammatory cells rather
55 than their activation state.

56 **Keywords:** ALS, AD, MS, TSPO, microglia

57 Introduction

58 Neuronal-microglial signalling limits microglial inflammatory responses under
59 homeostatic conditions¹. The loss of this cross talk in central nervous system (CNS)
60 pathology partly explains why microglia adopt an activated phenotype in many
61 neurodegenerative diseases^{2,3}. Genomic, *ex vivo* and preclinical data imply that microglial
62 activation also may contribute to neurodegeneration⁴, for example, by releasing
63 inflammatory molecules in response to infectious or damage-related triggers⁵. These lead
64 to both neuronal injury and, more directly, pathological phagocytosis of synapses^{5, 6}.
65 Development of tools which can reliably detect and quantify microglial activation in the
66 living human brain has been an important goal. By enabling improved stratification and
67 providing early pharmacodynamic readouts, these would accelerate experimental
68 medicine studies probing disease mechanisms and early therapeutics.

69 Detection of 18kDa Translocator Protein (TSPO) with positron emission tomography
70 (PET) has been widely used to quantify microglial activation *in vivo*⁷. In the last 5 years
71 alone, there have been ~300 clinical studies using TSPO PET to quantify microglial
72 responses in the human brain, making it the most commonly used research imaging
73 technique for this purpose.

74 The TSPO signal is not specific to microglia, and the contribution from other cell types
75 (particularly astrocytes and endothelial cells) is increasingly acknowledged⁸. The
76 justification for quantifying TSPO as a marker of microglial activation is based on the
77 assumption that when microglia become activated, they adopt a classical pro-
78 inflammatory phenotype and TSPO expression is substantially increased^{7, 9, 10}. This has
79 been demonstrated repeatedly in mice, both *in vitro* and *in vivo*¹¹⁻¹⁴. We have shown,
80 however, that classical proinflammatory stimulation of human microglia and
81 macrophages *in vitro* with the TLR4 ligand lipopolysaccharide (LPS) does not induce
82 expression of TSPO¹⁵. Furthermore, in multiple sclerosis (MS), TSPO does not appear to
83 be increased in microglia with activated morphology¹⁶. These data appear inconsistent
84 with the assumption that TSPO is a marker of activated microglia in humans.

85 To address this issue, we performed a meta-analysis of publicly available expression
86 array data and found that across a range of pro-inflammatory activation stimuli, TSPO
87 expression is consistently and substantially increased in mouse, but not human
88 macrophages and microglia *in vitro*. We then performed a comparative analysis of the
89 TSPO promoter region in a range of mammalian species and found that the binding site
90 for AP1 (a transcription factor which regulates macrophage activation in rats¹⁷) is
91 present in and unique to a subset of species within the *Muroidea* superfamily of rodents.
92 Consistent with the hypothesis that this binding site is required for the increase in TSPO
93 expression that accompanies pro-inflammatory stimulation, we show that TSPO is
94 inducible by LPS in the rat (another *Muroidea* species with the AP1 binding site in the
95 TSPO core promoter) but not in other mammals. Because neuronal interactions modulate
96 microglial phenotype, we then compared microglial TSPO expression in

97 neurodegenerative diseases affecting the brain and spinal cord (Alzheimer's Disease (AD)
98 and amyotrophic lateral sclerosis (ALS), respectively) as well as the classical
99 neuroinflammatory brain disease MS which features highly activated microglia. We
100 compared each human disease to its respective commonly used mouse models (amyloid
101 precursor protein (*App^{NL-G-F}*)¹⁸, tau (*Tau^{P301S}*)¹⁹, superoxide dismutase 1 (*SOD1^{G93A}*)²⁰,
102 and experimental autoimmune encephalomyelitis (EAE) in young and aged animals²¹. We
103 also studied TSPO expression with EAE in the marmoset in conjunction with frequent MRI
104 scanning that allowed for identification of the acute lesions which contain pro-
105 inflammatory microglia. Consistent with the *in vitro* data, we show that in AD, ALS and
106 MS, and in marmoset EAE, TSPO protein expression does not increase in CNS myeloid
107 cells that express a pro-inflammatory phenotype, while expression is markedly increased
108 in activated myeloid cells in all mouse models of these diseases. Finally, with exploration
109 of the relative expression of TSPO in publicly available CNS single cell RNA sequencing
110 (scRNAseq) data from brains of the human diseases and rodent models, we again show
111 an increase in microglial TSPO gene expression in mice with proinflammatory stimuli, but
112 not humans.

113 These data suggest that the commonly held assumption that TSPO PET is sensitive to
114 microglial *activation* is true only for a subset of species within the *Muroidea* superfamily
115 of rodents. In contrast, in humans and other mammals, it simply reflects the local density
116 of inflammatory cells irrespective of the disease context. The clinical interpretation of the
117 TSPO PET signal therefore needs to be revised.

118 **Results**

119 ***TSPO* expression and epigenetic regulation in primary macrophages**

120 To investigate *TSPO* gene expression changes in human and mice a meta-analysis was
121 performed using publicly available macrophage and microglia transcriptomic datasets
122 upon pro-inflammatory stimulation (Fig. 1). We found 10 datasets (Fig. 1a) derived from
123 mouse macrophages and microglia in samples from 68 mice and with inflammatory
124 stimuli including activation with LPS, Type 1 interferon (IFN), IFN γ , and LPS plus IFN γ .
125 We performed a meta-analysis and found that *Tspo* was upregulated under pro-
126 inflammatory conditions (Fig. 1a). In the individual datasets, *Tspo* was significantly
127 upregulated in 9 of the 10 experiments. We then interrogated 42 datasets from primary
128 human macrophages and microglia involving samples from 312 participants, with stimuli
129 including inflammatory activation with LPS, IFN γ , IL1, IL6, PolyIC, viruses, and bacteria
130 (Fig. 1b). In the meta-analysis, there was a non-significant trend towards a *reduction in*
131 human *TSPO* expression under pro-inflammatory conditions (Fig. 1b). In the individual
132 datasets, *TSPO* was unchanged in 33/42 (79%) of the datasets, significantly
133 downregulated in 8/42 (19%) and significantly upregulated in 1/42 (2%). In contrast to
134 the findings in mice, our analysis thus suggests that TSPO expression is not upregulated
135 in human microglia and macrophages after pro-inflammatory stimulation *in vitro*.

136 To test whether *TSPO* gene expression changes are regulated at an epigenetic level, we
137 analysed publicly available ChIP-seq datasets for histone modification in mouse and
138 human macrophages before and after treatment with IFN γ ^{22, 23} (Fig. 1c-f). Levels of
139 H3K27Ac and H3K4me1 histone marks in the enhancer regions are associated with
140 increased gene expression^{22, 24}. While both histone modifications were increased after
141 IFN γ treatment in *TSPO* promoter regions in macrophages from mouse, they were
142 decreased in humans (Fig. 1c,d). Consistent with this epigenetic regulation, *Tspo* gene
143 expression was upregulated in mouse macrophages after IFN γ but not in human
144 macrophages in RNAseq data from the same set of samples (Fig. S1a).

145 The PU.1 transcription factor is a master regulator of macrophage proliferation and
146 macrophage differentiation^{25, 26}. Because PU.1 increases *Tspo* gene expression in the
147 immortalised C57/BL6 mouse microglia BV-2 cell line²⁷, we next investigated whether
148 *TSPO* expression in macrophages is regulated by PU.1 binding in human in publicly
149 available ChIP-seq datasets. An increase in PU.1 binding in the mouse *Tspo* promoter after
150 IFN γ treatment was observed (Fig. 1c). However, PU.1 binding to the human *TSPO*
151 promoter was decreased after IFN γ treatment (Fig. 1d). To test whether the reduced PU.1
152 binding at the human *TSPO* promoter was due to reduced PU.1 expression, we analysed
153 RNAseq data from the same set of samples. Expression of SPI-1, the gene that codes for
154 PU.1, was not altered in human macrophages after IFN γ treatment (Fig. S1b), suggesting
155 that the reduced binding of PU.1 to the human *TSPO* promoter region was unlikely to be
156 due to reduced PU.1 levels. This suggests that repressive chromatin remodelling in the
157 human cells leads to decreased PU.1 binding, a consequence of which could be the
158 downregulation of *TSPO* transcript expression. This is consistent with the meta-analysis
159 (Fig. 1a,b); although *TSPO* expression with inflammatory stimuli did not significantly
160 change in most studies, in 8/9 (89%) of studies where *TSPO* did significantly change, it
161 was downregulated (Fig. 1b). Together this data shows that *in vitro*, pro-inflammatory
162 stimulation of mouse myeloid cells increases *TSPO* expression, histone marks in the
163 enhancer regions and PU.1 binding. These changes are not found following pro-
164 inflammatory stimulation of human myeloid cells.

165 **The presence of the AP1 binding site in the *TSPO* promoter and LPS inducible** 166 ***TSPO* expression is unique to the *Muroidea* superfamily of rodents**

167 To understand why *TSPO* expression is inducible by pro-inflammatory stimuli in mouse
168 but not human myeloid cells, we performed multiple sequence alignment of the *TSPO*
169 promoter region of 15 species including primates, rodents, and other mammals (Fig. 2).
170 We found that an AP1 binding site is present uniquely in a subset of species within the
171 *Muroidea* superfamily of rodents including mouse, rat and chinese hamster (Fig. 2a).
172 These binding sites were not present in other rodents (squirrel, guinea pig), nor in other
173 non-rodent mammals (Fig. 2a). We generated a phylogenetic tree which shows a clear
174 branching in the *TSPO* promoter of rat, mouse and chinese hamster from the other
175 rodents and non-rodent mammals (Fig. 2b). Differential motif enrichment analysis of the

176 TSPO promotor region between *Muroidea* vs non-*Muroidea* species confirmed a
177 significant enrichment of the AP1 binding site in the *Muroidea* promoter (Fig. 2c). We
178 expanded this motif search and *TSPO* promoter sequence divergence analysis to a wider
179 range of 24 rodent species from the *Muroidea* superfamily and other non-*Muroidea*
180 rodents. Again, we found that the AP1 site is confined only to a subset of the superfamily
181 *Muroidea* (Fig. S2).

182 Silencing AP1 impairs LPS induced TSPO expression in the immortalized mouse BV2 cell
183 line²⁷. We therefore tested the hypothesis that LPS inducible TSPO expression occurs only
184 in species with the AP1 binding site in the promoter region. In species that lack the AP1
185 binding site (human, pig, sheep, rabbit), TSPO expression was not induced by LPS (Fig.
186 2d). However, in the rat, where the AP1 binding site is present, TSPO was increased under
187 these conditions (Fig. 2d).

188 **Microglial TSPO expression is unchanged in the AD hippocampus, but is** 189 **increased in amyloid mouse models**

190 Microglia-neuronal interactions, which modulate microglia inflammatory phenotype¹,
191 are lost in monocultures *in vitro*. We therefore examined TSPO expression within
192 inflammatory microglia *in situ* with quantitative neuropathology using *postmortem*
193 samples from AD (Table S1). We compared data from human *postmortem* AD brain to the
194 *App^{NL-G-F}* and *TAU^{P301S}* mouse models.

195 We examined the hippocampal region, one of the most severely affected regions in AD²⁸,
196 ²⁹, comparing it to non-neurological disease controls (Fig. 3a-c). No increases were
197 observed in the number of IBA1+ microglia (Fig. 3d), HLA-DR+ microglia (Fig. 3e) or
198 astrocytes (Fig. 3f) and the density of TSPO+ cells in AD did not differ compared to
199 controls (Fig. 3g). Additionally, there was no increase in TSPO+ microglia (Fig. 3h,i) and
200 astrocytes (Fig. 3j). We then quantified TSPO+ area (μm^2) in microglia and astrocytes as
201 an index of individual cellular expression (see methods). There was no difference in
202 individual cellular TSPO expression in microglia (Fig. 3k) or astrocytes (Fig. 3k) in AD
203 relative to controls.

204 We next conducted multiplexed proteomics with imaging mass cytometry (IMC) for
205 further characterisation of cellular phenotype. As with the IHC, we did not see an increase
206 in microglial density, as defined by the number of IBA1+ cells per mm^2 , (Fig. S3a) nor in
207 the density of astrocytes (Fig. S3b). Furthermore, again in agreement with the IHC, we did
208 not see an increase in the number of microglia and astrocytes expressing TSPO (Fig.
209 S3c,d). However, IMC did reveal an increase in CD68+ microglia cells (Fig S3e) in AD
210 compared to control, providing evidence, consistent with the literature^{30, 31}, that
211 microglia are activated in AD. However, despite microglial activation, we did not find an
212 increase in individual cellular TSPO expression, defined here as mean cellular TSPO
213 signal, in either microglia (Fig. S3f) or astrocytes (Fig. S3g) in AD donors relative to
214 control. Because proximity to amyloid plaques is associated with activation of

215 microglia³⁰, we next tested whether cellular TSPO expression was higher in plaque
216 microglia relative to (more distant) non-plaque microglia in the same tissue sections
217 from the AD brains only. We saw no differences in cellular TSPO expression between the
218 plaque and non-plaque microglia (Fig. S3h).

219 We next compared the human AD data to that from mouse *App*^{NL-G-F} (Fig. 4a,b) and
220 TAU^{P301S} (Fig. 4,i,j). The *App*^{NL-G-F} model avoids artefacts introduced by APP
221 overexpression by utilising a knock-in strategy to express human APP at wild-type levels
222 and with appropriate cell-type and temporal specificity¹⁸. In this model, APP is not
223 overexpressed. Instead, amyloid plaque density is elevated due to the combined effects
224 of three mutations associated with familial AD (NL; Swedish, G: Arctic, F: Iberian). The
225 *App*^{NL-G-F} line is characterised by formation of amyloid plaques, microgliosis and
226 astrocytosis¹⁸. We also investigated TSPO expression in a model of tauopathy, TAU^{P301S}
227 mice, which develop tangle-like inclusions in the brain parenchyma associated with
228 microgliosis and astrocytosis¹⁹. The use of these two models allows differentiation of
229 effects of the amyloid plaques and neurofibrillary tangles on the expression of TSPO in
230 the mouse hippocampus. In *App*^{NL-G-F} mice, an increase in the density of microglia was
231 observed at 28-weeks (Fig. 4c), but not in the density of astrocytes (Fig. 4d). An increase
232 in TSPO+ cells was also observed (Fig. 4e), due to an increase in numbers of TSPO+
233 microglia and macrophages (Fig. 4f). No differences were observed in the density of
234 TSPO+ astrocytes in *App*^{NL-G-F} at 10 weeks, although a small (relative to that with
235 microglia) increase was observed at 28 weeks (Fig. 4g). Finally, we then quantified TSPO+
236 area in microglia and astrocytes as an index of TSPO expression in individual cells. In
237 contrast to the human data, expression of TSPO in individual cells was increased by 3-
238 fold in microglia in the *App*^{NL-G-F} mice at 28 weeks (Fig. 4h). It was unchanged in
239 astrocytes. In the TAU^{P301S} mice, no differences were observed in microglia (Fig. 4k) or
240 astrocyte (Fig. 4l) densities, in TSPO+ cell density (Fig. 4m), or in the density of TSPO+
241 microglia (Fig. 4n) or of TSPO+ astrocytes (Fig. 4o) in the hippocampus at either 8 or 20
242 weeks (Fig. 4). However, as with the *App*^{NL-G-F} mouse (and in contrast to the human), a 2-
243 fold increase in individual cellular TSPO expression was observed within microglia in
244 TAU^{P301S} mice (Fig 4p). Again, as with the *App*^{NL-G-F} mouse, individual cellular TSPO
245 expression within astrocytes was unchanged.

246 In summary, we showed that TSPO cellular expression is increased within microglia from
247 *App*^{NL-G-F} and TAU^{P301S} mice, but not in microglia from AD tissue. TSPO was also
248 unchanged in astrocytes from both mouse models and the human disease.

249 **Microglial TSPO is upregulated in SOD1^{G93A} mice but not in ALS**

250 Spinal cord and brain microglia differ with respect to development, phenotype and
251 function³². We therefore next investigated ALS (Table S2), that primarily affects the spinal
252 cord rather than the brain. We compared this data to that from the commonly used
253 SOD1^{G93A} mouse model of ALS. TSPO expression was investigated in the ventral horn and
254 lateral columns of the spinal cord in cervical, thoracic, and lumbar regions (Fig. 5a-c). An

255 increase in microglia (Fig. 5d), HLA-DR⁺ microglia (Fig. 5e) and astrocytes (Fig. 5f) was
256 observed in human ALS spinal cord. The density of TSPO⁺ cells was increased by 2.5-fold
257 in ALS spinal cords across all regions when compared to controls (Fig. 5g). No additional
258 changes were found when stratifying the cohort based on disease duration or spinal cord
259 regions, white or grey matter, or spinal cord levels. In comparison to the controls, ALS
260 samples exhibited a 3-fold increase in the density of TSPO⁺ microglia (TSPO⁺IBA1⁺ cells,
261 Fig. 5h) and a 3-fold increase in TSPO⁺ activated microglia/macrophages (TSPO⁺HLA-
262 DR⁺ cells, Fig. 5i). A 2.5-fold increase in the density of TSPO⁺ astrocytes (TSPO⁺GFAP⁺
263 cells) was observed in ALS compared to control (Fig. 5j). We then quantified TSPO⁺ area
264 in microglia and astrocytes as an index of individual cellular TSPO expression (Fig. 5k).
265 No increase in TSPO⁺ area (μm^2) was found in microglia or astrocytes in ALS when
266 compared to control (Fig. 5k), implying that TSPO expression does not increase in
267 microglia or astrocytes with ALS.

268 SOD1^{G93A} mice express high levels of mutant SOD1 that initiates adult-onset
269 neurodegeneration of spinal cord motor neurons leading to paralysis, and as such these
270 mice have been used as a preclinical model for ALS²⁰. To determine the extent to which
271 TSPO⁺ cells were present in SOD1^{G93A} mice TSPO⁺ microglia and astrocytes were
272 quantified with immunohistochemistry in the white and grey matter of the spinal cord
273 (Fig. 6a,b). An increase was observed in the total number of microglia (Fig. 6c) and
274 astrocytes (Fig. 6d) in 16-week old SOD1^{G93A} mice but not in 10 week old animals (Fig.
275 6c,d). The density of TSPO⁺ cells was increased 2- to 3-fold in presymptomatic disease
276 (10 weeks) compared to non-transgenic littermate control mice in both white and grey
277 matter (Fig. 6e). Increases in the density of TSPO⁺IBA⁺ cells were not observed in
278 SOD1^{G93A} mice compared to control animals (Fig. 6f). However, a significant 8- to 15-fold
279 increase in the density of TSPO⁺GFAP⁺ astrocytes was observed in 10- and 16-week old
280 SOD1^{G93A} mice compared to 10- and 16-week old wild-type mice (Fig. 6g). Finally, we then
281 quantified TSPO⁺ area in microglia and astrocytes as an index of individual cellular TSPO
282 expression. In contrast to the human data, where there was no change in disease samples
283 relative to controls, expression of TSPO in individual cells was increased by 1.5-fold in
284 microglia in the rodent model. As with the *App*^{NL-G-F} and *TAU*^{P301S} mice above, TSPO
285 expression within astrocytes was unchanged (Fig. 6h).

286 In summary, consistent with the data from AD and relevant mouse models, we have
287 shown that TSPO expression is increased within microglia from SOD1^{G93A} mice, but not
288 increased in microglia from human ALS tissue. TSPO also was unchanged in astrocytes
289 from the SOD1^{G93A} mice and the human disease relatively to those in the healthy control
290 tissues.

291 **Increased myeloid cell TSPO expression is found in mouse EAE, but not in MS** 292 **or marmoset EAE**

293 Having found no evidence of increased TSPO expression in activated microglia in human
294 neurodegenerative diseases affecting the brain or spinal cord, we next examined MS as

295 an example of a classical neuroinflammatory disease characterised by microglia with a
296 highly activated pro-inflammatory phenotype. We compared data from human
297 *postmortem* MS brain (Table S3) to mice with EAE (Table S4). We also examined brain
298 tissue from marmoset EAE (Table S5), as *antemortem* MRI assessments in these animals
299 allow for identification of acute lesions which are highly inflammatory.

300 We previously defined TSPO cellular expression in MS^{16, 33}. HLA-DR⁺ microglia
301 expressing TSPO were increased up to 14-fold in active lesions compared to control³³,
302 and these microglia colocalised with CD68 and had lost homeostatic markers P2RY12 and
303 TMEM119, indicating an activated microglial state¹⁶. Here we quantified individual
304 cellular TSPO expression in both microglia and astrocytes by comparing cells in active
305 white matter lesions to white matter from control subjects. Consistent with the human
306 data from AD and ALS, there was no difference in TSPO expression in individual microglia
307 or astrocytes in MS compared to control tissue (Fig 7a-c).

308 We next investigated the relative levels of TSPO expression (Fig. 7d-l) in microglia and
309 astrocytes in acute EAE (aEAE), a commonly used experimental mouse model of MS^{21, 34}.
310 Neurodegenerative diseases typically occur in old age, whereas aEAE and the AD and ALS
311 relevant rodent models described above are induced in young mice. As age might affect
312 TSPO regulation³⁵, we also investigated TSPO expression in progressive EAE (PEAE), a
313 model where the pathology is induced in aged mice (12 months).

314 Increases in numbers of both microglia and astrocytes were observed in aEAE as well as
315 in PEAE mice compared to their respective young and old control groups (Fig. 7f,g).
316 Similarly, increases were observed in the number of TSPO⁺ microglia and TSPO⁺
317 astrocytes in both aEAE and PEAE relative to their respective controls (Fig. 7h-j). When
318 comparing the young control mice (aEAE controls) with the old control mice (PEAE
319 controls), no differences were observed in microglial and TSPO⁺ microglial density (Fig.
320 7f,i). Similarly, there was no difference in density of astrocytes or TSPO⁺ astrocytes
321 between these two control groups (Fig. 7g,j).

322 To investigate individual cellular TSPO expression, TSPO⁺ area was measured in
323 microglia and astrocytes. Individual microglia expressed 3-fold greater TSPO and 2-fold
324 greater TSPO in aEAE and PEAE respectively, relative to their control groups. The
325 individual cellular TSPO expression was not higher in microglia from young mice relative
326 to old mice. Again, as with the SOD1^{G93A}, *App*^{NL-G-F}, and TAU^{P301S} mice, individual cellular
327 TSPO expression within astrocytes was unchanged.

328 Finally, we investigated TSPO expression in EAE induced in the common marmoset
329 (*Callithus jacchus*) (Fig. S4, Fig. 7m-o), a non-human primate which, like humans, lacks
330 the AP1 binding site in the core promoter region of TSPO. Both the neural architecture
331 and the immune system of the marmoset are more similar to humans than are those of
332 the mouse³⁶⁻³⁸. Marmoset EAE therefore has features of the human disease which are not
333 seen in mouse EAE, such as perivenular white matter lesions identifiable by MRI, B cell

334 infiltration and CD8+ T cell involvement. Marmosets were scanned with MRI biweekly,
335 which allowed the ages of lesions to be determined and the identification of acute lesions
336 including pro-inflammatory microglia. In acute and subacute lesions, there was an
337 increase of up to 27-fold in the density of TSPO+ microglia relative to control (Fig. S4a-c)
338 and these microglia bore the hallmarks of pro-inflammatory activation. However, TSPO
339 expression in individual microglia, here defined as the percentage of TSPO+ pixels using
340 immunofluorescence, was not increased in acute or subacute lesions relative to control
341 (Fig. 7o).

342 In summary, and consistent with the AD and ALS data, we have shown that individual
343 cellular TSPO expression is increased in microglia in EAE in both young and aged mouse
344 models, but it is not increased in microglia from MS lesions nor marmoset EAE acute
345 lesions. Again, consistent with previous data, astrocytes did not show an increase in TSPO
346 expression in either MS or EAE.

347 **Single cell RNAseq shows *TSPO* gene expression is upregulated in activated** 348 **mouse microglia, but not in activated human microglia**

349 Methods for protein quantification by immunohistochemistry in *postmortem* brain are
350 semiquantitative and therefore we also assessed *ex vivo* species-specific TSPO gene
351 expression of microglial under pro-inflammatory conditions to add further confidence to
352 our findings. We employed publicly available human and mouse scRNAseq datasets³⁹⁻⁴⁴.
353 We first examined evidence for a pro-inflammatory microglial phenotype by quantifying
354 the differential expression of homeostatic and/or activation markers. We then quantified
355 the differential expression of TSPO in pro-inflammatory activated microglia using
356 MAST⁴⁵.

357 In a model of LPS exposure in the mouse³⁹, scRNAseq yielded 2019 microglial cells that
358 showed evidence of pro-inflammatory activation including a downregulation of the
359 homeostatic marker *P2ry12* and an upregulation of activation markers *Fth1* and *Cd74*
360 (Fig. 9a). In this population, *TSPO* was significantly upregulated. In a mouse model of
361 acute EAE⁴⁰, scRNAseq yielded 8470 pro-inflammatory activated microglial cells that
362 showed significant downregulation of *P2ry12*, and a significant upregulation of *Fth1* and
363 *Cd74* (Fig. 9b). *TSPO* was significantly upregulated. Finally, in the 5XFAD mouse model of
364 AD⁴¹, scRNAseq yielded over 6203 microglial cells. Among them, 223 showed enrichment
365 in disease-associated microglia (DAM) markers⁴¹, including increased expression of *ApoE*,
366 *Trem2*, *Tyrobp* and *Cst7* (Fig. 9c). Compared to non-DAM cells, DAM cells showed a
367 significant upregulation of *TSPO*.

368 In cerebrospinal fluid (CSF)-derived cells isolated from people with AD⁴², microglia-like
369 cells (n=522) had an activated phenotype with a significant upregulation of *APOE*, *FTH1*
370 and *SPI1* relative to controls. However, *TSPO* was not differentially expressed (Fig. 9d). In
371 isolated from people with MS⁴³, microglia-like cells (n=4143) showed evidence of
372 activation: *CD74*, *CST3*, *HLA-DRA*, *HLA-DQA1* and *HLA-DPB1* all were significantly

373 upregulated⁴³. However, TSPO was significantly downregulated in these cells (Fig. 9e). In
374 a similarly designed study also using CSF-derived cells, microglia showing upregulation
375 of *HLA-DRB1*, *HLA-DRB5* and *SPI1* also downregulated TSPO⁴⁴ (Fig. 9f).

376 These experiments are consistent at the gene expression level with our own data at the
377 protein expression level showing that the *TSPO* gene is not increased in microglia in AD
378 or EAE, but is increased in their respective commonly used mouse models.

379 Discussion

380 Microglial activation accompanies and is a major contributor to neurodegenerative and
381 neuroinflammatory diseases^{1, 4-6, 46}. A better understanding of microglial activation in
382 combination with a technique that could reliably quantify activated microglia in the
383 human brain would have broad utility to monitor disease progression as well as response
384 to therapy. TSPO PET has been applied by many with this objective^{9, 10}. Here we have
385 tested the widely held assumption that *TSPO* cellular expression increases upon
386 microglial activation. We examined *in vitro* data from isolated myeloid cells across 6
387 species, multiple sequence alignment of the TSPO promoter region across 34 species, and
388 *ex vivo* neuropathological and scRNAseq data from human neuroinflammatory and
389 neurodegenerative diseases, with relevant marmoset and young and aged mouse models.
390 We show that TSPO expression increases in mouse and rat microglia when they are
391 activated by a range of stimuli, but that this phenomenon is unique to microglia from a
392 subset of species from the *Muroidea* superfamily of rodents. The increase in TSPO
393 expression is likely dependant on the AP1 binding site in the core promoter region of
394 TSPO.

395 This finding fundamentally alters the way in which the TSPO PET signal is interpreted,
396 because it implies that the microglial component of the TSPO PET signal reflects density
397 only, rather than a composite of density and activation phenotype. For example, in
398 Parkinson's Disease (PD) there is evidence of activated microglia in the *postmortem* brain
399 but minimal change in microglial density⁴⁷. Three well designed studies using modern
400 TSPO radiotracers found no difference in TSPO signal between PD and controls groups⁴⁸⁻
401 ⁵⁰. The lack of increase in the TSPO PET signal is consistent with the data presented here,
402 and should therefore not be interpreted as evidence for lack of microglial activation in
403 PD.

404 Our study has several limitations. First, we have only examined microglia under certain
405 pro-inflammatory conditions and cannot exclude the possibility that other stimulation
406 paradigms would increase TSPO in human myeloid cells. However, the *in vitro* stimuli
407 which were examined included a broad range of pro-inflammatory triggers, and the three
408 human diseases are diverse with respect to the mechanisms underlying the activation of
409 microglia. Second, the measurements of cellular TSPO expression we used in brain tissue
410 are semi-quantitative. However, the same IHC quantification methods were used in all
411 human and mouse comparisons, and these methods consistently detected cellular TSPO

412 increases in mouse microglia despite not detecting analogous changes in human
413 microglia. Furthermore, where IMC and immunofluorescence were used, the quantitative
414 data were consistent with IHC. The neuropathology protein quantification was also
415 consistent with gene expression measured by scRNAseq. Third, for RNAseq analysis, we
416 were restricted to single cell rather than single nucleus experiments. This is because *TSPO*
417 is detected in only 5-12% of microglial nuclei⁵¹⁻⁵⁴ but ~80% of microglial cells³⁹⁻⁴⁴.
418 Fourth, the *in vitro* assay which most closely mimics *in vivo* PET data is radioligand
419 binding, which quantifies the binding of the radioligand to the binding site itself. Here, we
420 quantified expression of the *TSPO* gene or protein rather than radioligand binding site
421 density. However, we have previously shown that for *TSPO*, gene expression, protein
422 expression and radioligand binding site data closely correlate¹⁵. Finally, whilst we
423 present data correlating inducible *TSPO* expression with the presence of the AP1 binding
424 site in the *TSPO* core promoter region, to demonstrate causation the AP1 binding site
425 would need to be knocked out from the mouse or rat, and knocked in to a non-*Muroidea*
426 rodent. Furthermore, although we were able to find array expression data for a range of
427 non-rodent mammals that show *TSPO* is not induced upon myeloid cell activation, we
428 were unable to find array expression data for those rodents that lack the AP1 binding site,
429 such as squirrel or naked mole rat.

430 In summary, we present *in vitro* expression and sequence alignment data from a range of
431 species, as well as *ex vivo* data from neurodegenerative and neuroinflammatory diseases
432 and associated animal models, showing that inflammation-induced increases in cellular
433 *TSPO* expression are restricted to microglia from a subset of species within the *Muroidea*
434 superfamily of rodents. This challenges the commonly held view that *TSPO* provides a
435 readout of microglial activation in the human brain and shows that the *TSPO* PET signal
436 likely reflects the local density of inflammatory cells irrespective of phenotype. The
437 interpretation of *TSPO* PET data therefore requires revision.

438 **Acknowledgements**

439 The authors thank the UK MS society for financial support (grant number: C008-16.1).
440 Raw count matrices corresponding to microglia-like cells from Ramesh et al.,⁴⁴ were
441 kindly provided by Prof Michael Wilson. DRO was funded by an MRC Clinician Scientist
442 Award (MR/N008219/1). PMM acknowledges generous support from Edmond J Safra
443 Foundation and Lily Safra, the NIHR Investigator programme and the UK Dementia
444 Research Institute. PMM and DRJO thank the Imperial College Healthcare Trust-NIHR
445 Biomedical Research Centre for infrastructure support and the Medical Research Council
446 for support of *TSPO* studies.

447 **Methods**

448 **Meta-analysis of *TSPO* gene expression.** Datasets were searched using the search
449 terms “Macrophage/Monocyte/Microglia” and filtered for ‘*Homo sapiens*’ and ‘*Mus*
450 *musculus*’. Datasets with accessible raw data and at least three biological replicates per

451 treatment group were used. To avoid microarray platform-based differences only
452 datasets with Affymetrix chip were used. Raw microarray datasets were downloaded
453 from ArrayExpress (<https://www.ebi.ac.uk/arrayexpress/>) and RMA normalisation was
454 used. The 'Limma' R package was used to compute differentially expressed genes, and the
455 resulting *P*-values are adjusted for multiple testing with Benjamini and Hochberg's
456 method to control the false discovery rate⁵⁵. Meta-analysis was performed using R
457 package 'meta'. A meta *P*-value was calculated using the random-effect model.

458 **ChIP-seq data processing and visualisation.** ChIP-seq datasets were downloaded from
459 GSE66594²² (human) and GSE38377⁵⁶ (mouse). Raw fastq sequences were aligned with
460 Bowtie⁵⁷ to the human reference genome hg19 or to mouse reference genome mm9,
461 annotated SAM files are converted to tag directories using HOMER⁵⁸ using the
462 makeTagDirectory module. These directories are further used for peak calling using -
463 style histone parameter or converted to the bigWig format normalized to 10⁶ total tag
464 counts with HOMER using the makeUCSCfile module with -fsize parameter set at 2e9. For
465 the analysis of histone ChIP-seq data input samples were utilized as control files during
466 peak detection, whereas IgG control files were used during peak correction of the PU.1
467 ChIP-seq data. Peaks were visualised using UCSC genome browser⁵⁹.

468 **Multiple sequence alignment and phylogenetic tree construction.** We have retrieved
469 the TSPO promoter region starting from 1 Kbp upstream and 500 bp downstream of the
470 putative transcription start site (TSS) of 35 rodent and non-rodent mammals from
471 ENSEMBL genome database (<http://www.ensembl.org/index.html>). The full list can be
472 found in the (Table X) The multiple sequence alignment was performed using the T-
473 Coffee (v 13.45.0.4846264) multiple sequencing tool with the parameter -
474 mode=procoffee which is specifically designed to align the promoter region^{60, 61}. The
475 sequence alignment and the phylogenetic tree were visualised using Jalview (v
476 2.11.1.6)⁶². Phylogenetic tree was constructed using MEGA11 using Maximum Parsimony
477 method with 1000 bootstrap replication. The MP tree was obtained using the Tree-
478 Bisection-Regrafting (TBR) algorithm⁶³.

479 **Motif finding and motif enrichment.** We have used SEA (Simple Enrichment Analysis)
480 from the MEME-suite (v 5.4.1) to calculate the relative motif enrichment between
481 Muroidea family species and non-Muroidea mammals^{64, 65}. We set the TSPO promoter
482 sequences for the three Muroidea species (Mouse, Rat, Chinese Hamster) as the input
483 sequence and the rest of species as the control sequence. We set the *E*-value ≤ 10 for
484 calculating significance. We used the motifs for AP1, ETS and SP1 from JASPAR motif
485 database (<https://jaspar.genereg.net/>).

486 **Multi-species TSPO expression in macrophage and microglia.** Datasets were
487 searched using the search terms "Macrophage/Monocyte", "Microglia" and "LPS". Dataset
488 featuring stimulation less than 3 hours were excluded. Datasets with accessible raw data
489 and at least three biological replicates were used. Microarray datasets were analysed as
490 the same way described in section "Meta-analysis of TSPO gene expression". Raw gene

491 count data for the RNAseq datasets were downloaded from either ArrayExpress or GEO
492 (<https://www.ncbi.nlm.nih.gov/geo/>) and differential expression was performed using
493 DESeq2⁶⁶. For S1a, the mouse *Tspo* expression (GEO ID: GSE38371) fold change was
494 directly used from the respective study since biological replicates were not publicly
495 accessible²³.

496 **Human Brain Tissue.** The rapid autopsy regimen of the Netherlands Brain Bank in
497 Amsterdam (coordinator Prof I. Huitinga) was used to acquire the samples. Human tissue
498 was obtained at autopsy from the spinal cord (cervical, thoracic, lumbar levels) from 12
499 ALS patients, 7 with short disease duration (SDD; <18 months survival; mean survival
500 11.1 ± 3.4 months) and 4 with medium disease duration (MDD; >24 months survival;
501 mean survival 71.5 ± 31.5 months). Tissues for controls were collected from 10 age-
502 matched cases with no neurological disorders or peripheral inflammation (Table S1). The
503 hippocampal region was collected from 5 AD patients with Braak stage 6, and 5 aged-
504 matched controls that had no cognitive impairments prior to death (Table S2). Active MS
505 lesions were obtained from 5 MS cases as well as white matter from age-matched controls
506 (Table S3). All tissue was collected with the approval of the Medical Ethical Committee of
507 the Amsterdam UMC. All participants or next of kin had given informed consent for
508 autopsy and use of their tissue for research purposes.

509 **Generation and details of mouse and marmoset models**

510 **Mouse EAE.** Spinal cord tissue from mice with EAE was obtained from Biozzi ABH mice
511 housed at Queen Mary University of London, UK (originally obtained from Harlan UK Ltd,
512 Bicester, UK). The mice were raised under pathogen-free conditions and showed a
513 uniform health status throughout the studies. EAE was induced via injection of mouse
514 spinal cord homogenate in complete Freund's adjuvant (CFA) into mice of 8-12 weeks or
515 12 months of age as described previously^{34, 67}. Immediately, and 24 h after injection mice
516 were given 200ng *Bordetella pertussis* toxin (PT). Age-matched control groups were
517 immunized with CFA and PT. Table S4 gives an overview of the EAE mice used in this
518 study, including a score of neurological signs (0 = normal, 1 = flaccid tail, 2 = impaired
519 righting reflex, 3 = partial hindlimb paresis, 4 = complete hindlimb paresis, 5 =
520 moribund). Spinal cord was collected from acute (aEAE)⁶⁷ in the young mice, and
521 progressive EAE (PEAE) in the 12 month old mice. Animal procedures complied with
522 national and institutional guidelines (UK Animals Scientific Procedures Act 1986) and
523 adhered to the 3R guidelines⁶⁸.

524 **Marmoset EAE.** EAE was induced by subcutaneous immunization with 0.2 g of white
525 matter homogenate emulsified in CFA in 3 adult common marmosets (*Callithrix jacchus*)
526 at 4 dorsal sites adjacent to inguinal and axillary lymph nodes. Animals were monitored
527 daily for clinical symptoms of EAE progression and assigned clinical EAE scores weekly
528 based on extent of disability. Neurological exams were performed by a neurologist prior
529 to each MRI scan. All animals discussed in this study are shown in Table S5. Animal #8
530 was treated with prednisolone for 5 days as part of a concurrent study (primary results

531 not yet published). These animals were the first within their twin pair that showed three
532 or more brain lesions by *in vivo* MRI and received corticosteroid treatment with the goal
533 to reduce the severity of inflammation and potentially allow longer-term evaluation of
534 the lesions. MRI analyses were performed according to previously published marmoset
535 imaging protocols using T1, T2, T2*, and PD-weighted sequences on a Bruker 7T animal
536 magnet⁶⁹. Marmosets were scanned biweekly over the course of the EAE study. Following
537 the completion of EAE studies, the brains, spinal cords, and optic nerves excised from
538 euthanized animals were scanned by MRI for *postmortem* characterization of brain
539 lesions and previously uncharacterized spinal lesions and optic nerve lesions. Animal
540 procedures complied with national and institutional guidelines (NIH, Bethesda, USA)

541 **SOD1^{G93A}**. Female hemizygous transgenic SOD1^{G93A} mice on 129SvHsd genetic
542 background (n=10) and corresponding non transgenic littermates (n=9) were used. This
543 mouse line was raised at the Mario Negri Institute for Pharmacological Research-IRCCS,
544 Milan, Italy, derived from the line (B6SJL-TgSOD1^{G93A}-1Gur, originally purchased from
545 Jackson Laboratories, USA) and maintained on a 129S2/SvHsd background⁷⁰. The
546 thoracic segments of spinal cord were collected from 10- and 16-week-old mice and
547 processed as previously described⁷¹. Briefly, anaesthetised mice were transcardially
548 perfused with 0.1M PBS followed by 4% PFA. The spinal cord was quickly dissected out
549 and left PFA overnight at 4°C, rinsed, and stored 24 h in 10% sucrose with 0.1% sodium
550 azide in 0.1 M PBS at 4°C for cryoprotection, before mounting in optimal cutting
551 temperature compound (OCT) and stored at -80°C.

552 Procedures involving animals and their care were conducted in conformity with the
553 following laws, regulations, and policies governing the care and use of laboratory
554 animals: Italian Governing Law (D.lgs 26/2014; Authorization 19/2008-A issued 6
555 March, 2008 by Ministry of Health); Mario Negri Institutional Regulations and Policies
556 providing internal authorization for persons conducting animal experiments; the
557 National Institutes of Health's Guide for the Care and Use of Laboratory Animals (2011
558 edition), and European Union directives and guidelines (EEC Council Directive,
559 2010/63/UE).

560 **APP^{NL-G-F}**. For the APP^{NL-G-F} model of AD, male and female brain tissue was obtained from
561 11 homozygous (APP^{NL-G-F/NL-G-F}) APP knock-in mice and 11 wild type mice. Mice were
562 bred at Charles River Laboratories, UK and sampled at the Imperial College London, UK.
563 Brain tissue samples were collected fresh from 10- and 28 week-old mice that were
564 euthanised with sodium pentobarbital and exsanguinated. Animal procedures complied
565 with national and institutional guidelines (UK Animals Scientific Procedures Act 1986)
566 and adhered to 3R guidelines. Hippocampal areas were used as region of interest for
567 characterization.

568 **Tau^{P301S}**. Male brain tissue was obtained from 10 homozygous P301S knock-in mice⁷²⁻⁷⁴
569 and 8 wild-type C57/Bl6-OLA mice (Envigo, UK) from the Centre for Clinical Brain
570 Sciences, Edinburgh, United Kingdom. Brain tissue samples were collected from 8- and

571 20-week-old mice that were perfused with PBS and 4% paraformaldehyde, with tissues
572 being post-fixed overnight before being cryopreserved in 30% sucrose and frozen
573 embedded in tissue tec (Leica, UK). Sections were cut, 20µm, on a cryostat onto
574 superfrost plus slides and stored in -80 freezer. Animal procedures complied with
575 national and institutional guidelines (UK Animals Scientific Procedures Act 1986 &
576 University of Edinburgh Animal Care Committees) and adhered to 3R guidelines.
577 Hippocampal areas were used as region of interest for characterization.

578 For all studies mice were housed 4-5 per standard cages in specific pathogen-free and
579 controlled environmental conditions (temperature: 22±2°C; relative humidity: 55±10%
580 and 12 h of light/dark). Food (standard pellets) and water were supplied *ad libitum*.

581 **Immunohistochemistry.** Paraffin sections were de-paraffinized by immersion in xylene
582 for 5 min and rehydrated in descending concentrations of ethanol and fixed-frozen
583 sections were dried overnight. After washing in PBS, endogenous peroxidase activity was
584 blocked with 0.3 % H₂O₂ in PBS while for immunofluorescence sections were incubated
585 in 0.1% glycine. Antigen retrieval was performed with citrate or TRIS/EDTA buffer,
586 depending on the antibody, in a microwave for 3 min at 1000W and 10 min at 180W.
587 Sections were cooled down to RT and incubated with primary antibodies (Table S6)
588 diluted in antibody diluent (Sigma, U3510) overnight. Sections were washed with PBS
589 and afterwards incubated with the appropriate secondary antibodies for 1 h at room
590 temperature. HRP labelled antibodies were developed with diluted 3,3'-
591 diaminobenzidine (DAB; 1:50, DAKO) for 10 min and counterstained with haematoxylin.
592 Sections were immersed in ascending ethanol solutions and xylene for dehydration and
593 mounted with Quick-D. For immunofluorescence, sections were incubated with Alexa
594 Fluor®-labelled secondary antibodies. Autofluorescent background signal was reduced
595 by incubating sections in Sudan black (0.1% in 70% EtOH) for 10 min. Nuclei were stained
596 with 4,6-diamidino-2-phenylindole (DAPI) and slides were mounted onto glass
597 coverslips with Fluoromount™ (Merck).

598 **Imaging mass cytometry.** Antibody conjugation was performed using the Maxpar X8
599 protocol (Fluidigm). 51 slides of paraffin-embedded tissue from the Medial Temporal
600 Gyrus (MTG) and 48 slides of paraffin-embedded tissue from the Somatosensory Cortex
601 (SSC) underwent IMC staining and ablation. Each slide was within 5-10µm in thickness.
602 The slides underwent routine dewaxing and rehydration before undergoing antigen
603 retrieval, in a pH8 Ethylenediaminetetraacetic acid (EDTA) buffer. The slides were
604 blocked in 10% normal horse serum (Vector Laboratories) before incubation with a
605 conjugated-antibody cocktail (Table S6) at 4°C overnight. Slides were then treated in
606 0.02% Triton X-100 (Sigma-Aldrich) before incubation with an Iridium-intercalator
607 (Fluidigm) then washed in dH₂O and air-dried. Image acquisition took place using a
608 Hyperion Tissue Imager (Fluidigm) coupled to a Helios mass cytometer. The instrument
609 was tuned using the manufacturer's 3-Element Full Coverage Tuning Slide before the
610 slides were loaded into the device. 4 500x500µm regions of interest within the grey
611 matter were selected and then ablated using a laser at a frequency of 200Hz at a 1µm

612 resolution. The data was stored as .mcd files compatible with MCD Viewer software
613 (Fluidigm) then exported as TIFF files. Post-acquisition image processing using ImageJ
614 (v1.53c) software allowed threshold correction and the despeckle function to reduce
615 background noise. The data was opened with HistoCAT (BodenmillerGroup) to quantify
616 the signal of each Ln-channel and exported as .csv files.

617 **Multiplex immunofluorescence.** To immunophenotype microglia/macrophages
618 expressing TSPO in the marmoset CNS, a multi-color multiplex immunofluorescence
619 panel was used to stain for Iba1, PLP, and TSPO. Deparaffinised sections were washed
620 twice in PBS supplemented with 1 mg/ml BSA (PBS/BSA), followed by two washes in
621 distilled water. Antigen retrieval was performed by boiling the slide in 10mM citrate
622 buffer (pH 6) for 10 min in an 800W microwave at maximum power, after which they
623 were allowed to cool for 30 min and washed twice in distilled water. To reduce
624 nonspecific Fc receptor binding, the section was incubated in 250 μ l of FcR blocker
625 (Innovex Biosciences, cat. no. NB309) for 15 min at room temperature and washed twice
626 in distilled water. To further reduce background, sections were coated with 250 μ l
627 Background Buster (Innovex Biosciences, cat. no. NB306) for 15 min at room
628 temperature and washed twice in distilled water. Sections were incubated for 45 min at
629 room temperature in a primary antibody cocktail containing antibodies diluted in
630 PBS/BSA (Supplemental Table 1), washed in PBS/BSA and three changes of distilled
631 water. They were then incubated for 45 min in a secondary antibody cocktail composed
632 of secondary antibodies diluted in PBS/BSA containing DAPI (Invitrogen, cat. no. D1306,
633 100 ng/ml) (Supplemental Table 2), then washed once in PBS/BSA and twice in distilled
634 water. To facilitate mounting, the sections were air-dried for 15 min at room
635 temperature, sealed with a coverslip as described previously, and allowed to dry
636 overnight prior to image acquisition.

637 **Imaging and statistical analyses.** Brightfield images were collected at 40x
638 magnification using a Leica DC500 microscope (Leica Microsystems, Heidelberg,
639 Germany, Japan), or a Leica DM6000 (Leica Microsystems, Heidelberg, Germany) or a
640 Zeiss AxioImager.Z2 wide field scanning microscope for fluorescent images. For AD,
641 APP^{NL-G-F}, and TAU^{P301S} tissue images were collected from the hippocampus. For ALS
642 tissue, images of the ventral horn and the lateral column were obtained from cervical,
643 thoracic, and lumbar spinal cord levels. For mouse EAE and SOD1^{G93A} mice, images of grey
644 and white matter of the spinal cord were collected per case. ImageJ software was used
645 for picture analyses. Nuclei and stained cells were counted manually using the cell
646 counter plugin (de Vos, University of Sheffield, UK), excluding nuclei at the rim of each
647 picture and within blood vessels. To determine inter-observer variation 18 pictures were
648 manually counted by 3 independent observers with a correlation coefficient of > 0.9. To
649 determine single cell TSPO expression, IBA+ or GFAP+ cells were outlined manually using
650 the imageJ using the ROI manager. Afterwards TSPO+ pixels were measured within IBA+
651 and GFAP+ ROIs per cell. Data were analyzed using GraphPad Prism 9.1.0 software. All
652 data were tested for normal distribution, using the Shapiro-Wilk normality test.

653 Significant differences were detected using an unpaired t-test or one-way analysis of
654 variance test. Dunnett's post-hoc test was performed to analyze which groups differ
655 significantly. Number of mice were calculated by power analysis and as a maximum 6-8
656 mice were used per group based on previous studies³⁴. Data was considered significant
657 when $P < 0.05$.

658 **Human and mouse scRNAseq analysis of microglia.** We assessed alterations in gene
659 expression of *TSPO* in human and mouse activated microglia in publicly available
660 scRNAseq datasets. *Postmortem* human brain samples are predominantly studied using
661 single *nucleus* RNA sequencing (snRNAseq) rather than single *cell* RNAseq (sc)RNAseq
662 because the latter requires intact cells which cannot be recovered from frozen brain
663 tissue samples. However, *TSPO* is detected in a very low percentage of nuclei from
664 snRNAseq experiments which prevents accurate assessment of differential expression of
665 *TSPO* across disease or microglial states⁵⁴. For this reason, we searched MEDLINE for
666 human scRNAseq experiments involving AD, MS and ALS donors and mouse brain
667 scRNAseq datasets derived from the respective mouse models, as well as of pro-
668 inflammatory activation with LPS treatment. We found three human studies involving
669 donors with AD⁴² and MS^{43, 44}. Where microglia from CSF samples were analysed with
670 scRNAseq. We found no studies with ALS donors. We found three mouse studies: an LPS
671 activated model³⁹ an AD model⁴¹ and acute EAE⁴⁰. A fourth mouse scRNAseq dataset was
672 identified from LPS-treated mice⁷⁵, however, due to its small size (less than 400
673 microglial cells were sequenced), this dataset was discarded from further analysis. Raw
674 count matrices were downloaded from the Gene Expression Omnibus (GEO) with the
675 following accession numbers: GSE130119⁴⁰, GSE115571³⁹, GSE98969⁴¹, GSE138266⁴³
676 and GSE134578⁴². Data were processed with Seurat (v3)⁷⁶ or nf-core/scflow⁷⁷. Quality
677 control, sample integration, dimension reduction and clustering were performed using
678 default parameters as previously described^{54, 78}. Microglial cells (mouse datasets) and
679 microglia-like cells were identified using previously described cell markers. Differential
680 gene expression analysis was performed using MAST⁴⁵ implemented in Seurat to perform
681 zero-inflated regression analysis by fitting a fixed-effects model. Disease vs control group
682 comparisons were performed for all datasets, except for the Keren-Shaul dataset where
683 the AD-associated microglia phenotype was compared to the rest of the microglial
684 population in 5XFAD mice. In all cases, we assessed expression of activated microglial
685 markers. Gene expression alterations were considered significant when the adjusted p
686 value was equal to or lower than 0.05.

687 **Reporting Summary**

688 Further information on research design is available in the Nature Research Reporting
689 Summary linked to this article.

690 **Data availability**

691 The data that support the findings of this study are available in this manuscript and the
692 Supplementary Information. Source data are provided with this paper.

693 **Code availability**

694 Code used throughout this study is available upon request from the corresponding
695 authors.

696 **Author contributions**

697 Conceptualisation: E.N., N.F., S.A., and D.R.O. Technical and Analysis Support: J.A., D.S., S.C.,
698 M.C.T., T.Saito., T.Saido., M.W., C.S.M., C.B., and C.I.R. Data Collection and Curation: E.N.,
699 N.F., M.C.M., S.T., R.C.J.M., I.F., J.B., D.H., and R.P. Writing – Original Draft: E.N., N.F., S.A.,
700 and D.R.O. Writing – Review and Editing: All authors have reviewed the manuscript.
701 Visualisation: E.N., N.F., M.C.M., S.T., R.C.J.M., and I.F. Supervision: S.A., and D.R.O.

702 **References**

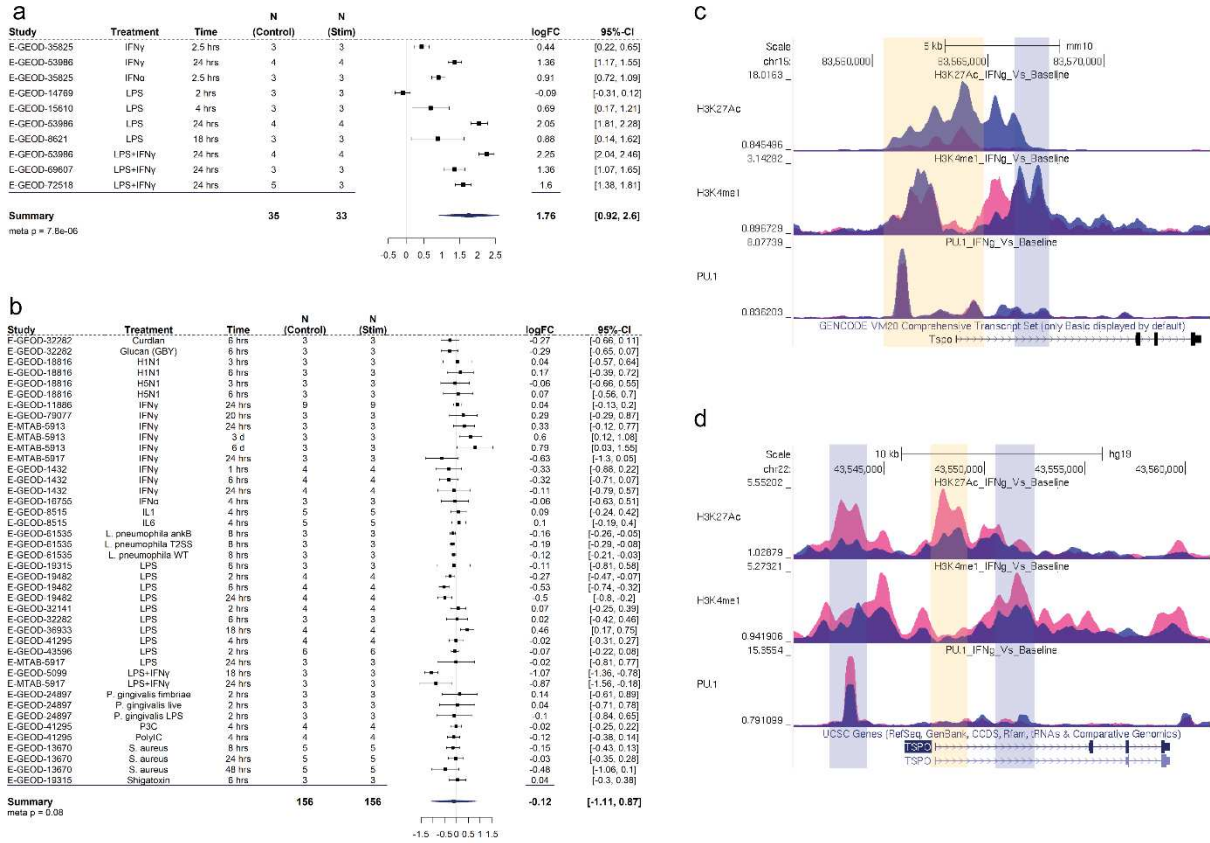
- 703 1. Cunningham , C. Microglia and neurodegeneration: the role of systemic inflammation. *Glia* **61**, 71-90
704 (2013).
- 705 2. Heneka, M.T., *et al.* Locus ceruleus controls Alzheimer's disease pathology by modulating microglial
706 functions through norepinephrine. *Proc Natl Acad Sci U S A* **107**, 6058-6063 (2010).
- 707 3. O'Sullivan, J.B., Ryan, K.M., Curtin, N.M., Harkin, A. & Connor, T.J. Noradrenaline reuptake inhibitors
708 limit neuroinflammation in rat cortex following a systemic inflammatory challenge: implications for
709 depression and neurodegeneration. *Int J Neuropsychopharmacol* **12**, 687-699 (2009).
- 710 4. Brown, G.C. & Vilalta, A. How microglia kill neurons. *Brain Res* **1628**, 288-297 (2015).
- 711 5. Brown, G.C. & Neher, J.J. Inflammatory neurodegeneration and mechanisms of microglial killing of
712 neurons. *Mol Neurobiol* **41**, 242-247 (2010).
- 713 6. Brown, G.C. & Neher, J.J. Microglial phagocytosis of live neurons. *Nature reviews. Neuroscience* **15**, 209-
714 216 (2014).
- 715 7. Guilarte, T.R. TSPO in diverse CNS pathologies and psychiatric disease: A critical review and a way
716 forward. *Pharmacol Ther* **194**, 44-58 (2019).
- 717 8. Guilarte, T.R., Rodichkin, A.N., McGlothan, J.L., Acanda De La Rocha, A.M. & Azzam, D.J. Imaging
718 neuroinflammation with TSPO: A new perspective on the cellular sources and subcellular localization.
719 *Pharmacol Ther*, 108048 (2021).
- 720 9. Pascoal, T.A., *et al.* Microglial activation and tau propagate jointly across Braak stages. *Nature medicine*
721 **27**, 1592-1599 (2021).
- 722 10. Jucaite, A., *et al.* Effect of the myeloperoxidase inhibitor AZD3241 on microglia: a PET study in
723 Parkinson's disease. *Brain : a journal of neurology* **138**, 2687-2700 (2015).
- 724 11. Bae, K.R., Shim, H.J., Balu, D., Kim, S.R. & Yu, S.W. Translocator protein 18 kDa negatively regulates
725 inflammation in microglia. *J Neuroimmune Pharmacol* **9**, 424-437 (2014).
- 726 12. Wang, M., *et al.* Macroglia-microglia interactions via TSPO signaling regulates microglial activation in
727 the mouse retina. *J Neurosci* **34**, 3793-3806 (2014).
- 728 13. Karlstetter, M., *et al.* Translocator protein (18 kDa) (TSPO) is expressed in reactive retinal microglia
729 and modulates microglial inflammation and phagocytosis. *J Neuroinflammation* **11**, 3 (2014).
- 730 14. Gottfried-Blackmore, A., Sierra, A., Jellinck, P.H., McEwen, B.S. & Bulloch, K. Brain microglia express
731 steroid-converting enzymes in the mouse. *J Steroid Biochem Mol Biol* **109**, 96-107 (2008).
- 732 15. Owen, D.R., *et al.* Pro-inflammatory activation of primary microglia and macrophages increases 18 kDa
733 translocator protein expression in rodents but not humans. *J Cereb Blood Flow Metab* **37**, 2679-2690
734 (2017).

- 735 16. Nutma, E., *et al.* Activated microglia do not increase 18 kDa translocator protein (TSPO) expression in
736 the multiple sclerosis brain. *Glia* **69**, 2447-2458 (2021).
- 737 17. Srivastava, P.K., Hull, R.P., Behmoaras, J., Petretto, E. & Aitman, T.J. JunD/AP1 regulatory network
738 analysis during macrophage activation in a rat model of crescentic glomerulonephritis. *BMC Syst Biol*
739 **7**, 93 (2013).
- 740 18. Saito, T., *et al.* Single App knock-in mouse models of Alzheimer's disease. *Nature neuroscience* **17**, 661-
741 663 (2014).
- 742 19. Yoshiyama, Y., *et al.* Synapse loss and microglial activation precede tangles in a P301S tauopathy
743 mouse model. *Neuron* **53**, 337-351 (2007).
- 744 20. Gurney, M.E., *et al.* Motor neuron degeneration in mice that express a human Cu,Zn superoxide
745 dismutase mutation. *Science* **264**, 1772-1775 (1994).
- 746 21. Baker, D., *et al.* Induction of chronic relapsing experimental allergic encephalomyelitis in Biozzi mice.
747 *J Neuroimmunol* **28**, 261-270 (1990).
- 748 22. Schmidt, S.V., *et al.* The transcriptional regulator network of human inflammatory macrophages is
749 defined by open chromatin. *Cell Res* **26**, 151-170 (2016).
- 750 23. Ostuni, R., *et al.* Latent enhancers activated by stimulation in differentiated cells. *Cell* **152**, 157-171
751 (2013).
- 752 24. Shlyueva, D., Stampfel, G. & Stark, A. Transcriptional enhancers: from properties to genome-wide
753 predictions. *Nat Rev Genet* **15**, 272-286 (2014).
- 754 25. Celada, A., *et al.* The transcription factor PU.1 is involved in macrophage proliferation. *J Exp Med* **184**,
755 61-69 (1996).
- 756 26. Ghisletti, S., *et al.* Identification and characterization of enhancers controlling the inflammatory gene
757 expression program in macrophages. *Immunity* **32**, 317-328 (2010).
- 758 27. Rashid, K., Geissl, L., Wolf, A., Karlstetter, M. & Langmann, T. Transcriptional regulation of Translocator
759 protein (18kDa) (TSPO) in microglia requires Pu.1, Ap1 and Sp factors. *Biochim Biophys Acta Gene*
760 *Regul Mech* **1861**, 1119-1133 (2018).
- 761 28. Lane, C.A., Hardy, J. & Schott, J.M. Alzheimer's disease. *Eur J Neurol* **25**, 59-70 (2018).
- 762 29. Tiwari, S., Atluri, V., Kaushik, A., Yndart, A. & Nair, M. Alzheimer's disease: pathogenesis, diagnostics,
763 and therapeutics. *International journal of nanomedicine* **14**, 5541-5554 (2019).
- 764 30. Kellner, A., *et al.* Autoantibodies against beta-amyloid are common in Alzheimer's disease and help
765 control plaque burden. *Ann Neurol* **65**, 24-31 (2009).
- 766 31. Hansen, D.V., Hanson, J.E. & Sheng, M. Microglia in Alzheimer's disease. *J Cell Biol* **217**, 459-472 (2018).
- 767 32. Xuan, F.L., Chithanathan, K., Lillevali, K., Yuan, X. & Tian, L. Differences of Microglia in the Brain and
768 the Spinal Cord. *Front Cell Neurosci* **13**, 504 (2019).
- 769 33. Nutma, E., *et al.* A quantitative neuropathological assessment of translocator protein expression in
770 multiple sclerosis. *Brain : a journal of neurology* **142**, 3440-3455 (2019).
- 771 34. Peferoen, L.A., *et al.* Ageing and recurrent episodes of neuroinflammation promote progressive
772 experimental autoimmune encephalomyelitis in Biozzi ABH mice. *Immunology* **149**, 146-156 (2016).
- 773 35. Tuisku, J., *et al.* Effects of age, BMI and sex on the glial cell marker TSPO - a multicentre [(11)C]PBR28
774 HRRT PET study. *European journal of nuclear medicine and molecular imaging* **46**, 2329-2338 (2019).
- 775 36. Gaitan, M.I., *et al.* Perivenular brain lesions in a primate multiple sclerosis model at 7-tesla magnetic
776 resonance imaging. *Mult Scler* **20**, 64-71 (2014).
- 777 37. t Hart, B.A., Vogels, J., Bauer, J., Brok, H.P. & Blezer, E. Non-invasive measurement of brain damage in a
778 primate model of multiple sclerosis. *Trends Mol Med* **10**, 85-91 (2004).
- 779 38. Lefevre, J.A., *et al.* The spectrum of spinal cord lesions in a primate model of multiple sclerosis. *Mult*
780 *Scler* **26**, 284-293 (2020).
- 781 39. Sousa, C., *et al.* Single-cell transcriptomics reveals distinct inflammation-induced microglia signatures.
782 *EMBO Rep* **19**, e46171 (2018).
- 783 40. Wheeler, M.A., *et al.* MAFG-driven astrocytes promote CNS inflammation. *Nature* **578**, 593-599 (2020).
- 784 41. Keren-Shaul, H., *et al.* A Unique Microglia Type Associated with Restricting Development of
785 Alzheimer's Disease. *Cell* **169**, 1276-1290 e1217 (2017).
- 786 42. Gate, D., *et al.* Clonally expanded CD8 T cells patrol the cerebrospinal fluid in Alzheimer's disease.
787 *Nature* **577**, 399-404 (2020).
- 788 43. Schafflick, D., *et al.* Integrated single cell analysis of blood and cerebrospinal fluid leukocytes in
789 multiple sclerosis. *Nat Commun* **11**, 247 (2020).
- 790 44. Ramesh, A., *et al.* A pathogenic and clonally expanded B cell transcriptome in active multiple sclerosis.
791 *Proc Natl Acad Sci U S A* **117**, 22932-22943 (2020).
- 792 45. Finak, G., *et al.* MAST: a flexible statistical framework for assessing transcriptional changes and
793 characterizing heterogeneity in single-cell RNA sequencing data. *Genome Biol* **16**, 278 (2015).

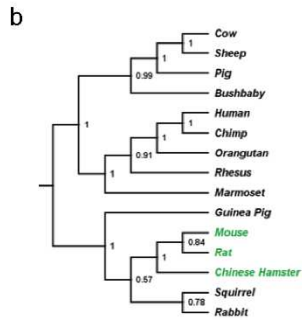
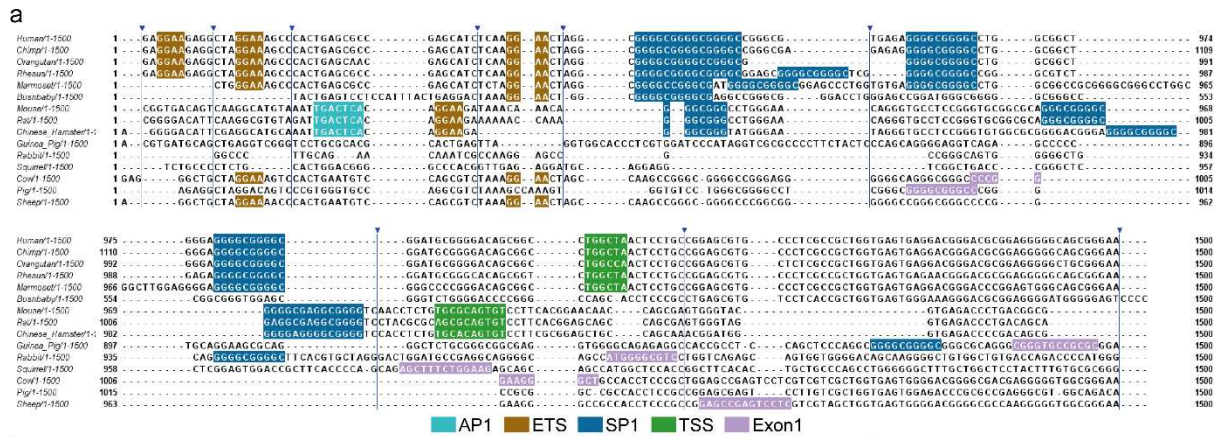
- 794 46. Stephenson, J., Nutma, E., van der Valk, P. & Amor, S. Inflammation in CNS neurodegenerative diseases. *Immunology* **154**, 204-219 (2018).
795
796 47. Doorn, K.J., *et al.* Microglial phenotypes and toll-like receptor 2 in the substantia nigra and
797 hippocampus of incidental Lewy body disease cases and Parkinson's disease patients. *Acta*
798 *neuropathologica communications* **2**, 90 (2014).
799 48. Ghadery, C., *et al.* Microglial activation in Parkinson's disease using [(18)F]-FEPPA. *J*
800 *Neuroinflammation* **14**, 8 (2017).
801 49. Koshimori, Y., *et al.* Imaging Striatal Microglial Activation in Patients with Parkinson's Disease. *PLoS*
802 *One* **10**, e0138721 (2015).
803 50. Varnäs, K., *et al.* PET imaging of [11C] PBR28 in Parkinson's disease patients does not indicate
804 increased binding to TSPO despite reduced dopamine transporter binding. *European journal of nuclear*
805 *medicine and molecular imaging* **46**, 367-375 (2019).
806 51. Mathys, H., *et al.* Author Correction: Single-cell transcriptomic analysis of Alzheimer's disease. *Nature*
807 **571**, E1 (2019).
808 52. Grubman, A., *et al.* A single-cell atlas of entorhinal cortex from individuals with Alzheimer's disease
809 reveals cell-type-specific gene expression regulation. *Nature neuroscience* **22**, 2087-2097 (2019).
810 53. Zhou, Y., *et al.* Human and mouse single-nucleus transcriptomics reveal TREM2-dependent and
811 TREM2-independent cellular responses in Alzheimer's disease. *Nature medicine* **26**, 131-142 (2020).
812 54. Smith, A.M., *et al.* Diverse human astrocyte and microglial transcriptional responses to Alzheimer's
813 pathology. *Acta Neuropathol* (2021).
814 55. Benjamini, Y. & Hochberg, Y. Controlling the False Discovery Rate - a Practical and Powerful Approach
815 to Multiple Testing. *J R Stat Soc B* **57**, 289-300 (1995).
816 56. Felton, J.M., *et al.* Epigenetic Analysis of the Chromatin Landscape Identifies a Repertoire of Murine
817 Eosinophil-Specific PU.1-Bound Enhancers. *J Immunol* **207**, 1044-1054 (2021).
818 57. Langmead, B., Trapnell, C., Pop, M. & Salzberg, S.L. Ultrafast and memory-efficient alignment of short
819 DNA sequences to the human genome. *Genome Biol* **10**, R25 (2009).
820 58. Heinz, S., *et al.* Simple combinations of lineage-determining transcription factors prime cis-regulatory
821 elements required for macrophage and B cell identities. *Mol Cell* **38**, 576-589 (2010).
822 59. Kent, W.J., *et al.* The human genome browser at UCSC. *Genome Res* **12**, 996-1006 (2002).
823 60. Notredame, C., Higgins, D.G. & Heringa, J. T-Coffee: A novel method for fast and accurate multiple
824 sequence alignment. *J Mol Biol* **302**, 205-217 (2000).
825 61. Erb, I., *et al.* Use of ChIP-Seq data for the design of a multiple promoter-alignment method. *Nucleic*
826 *Acids Research* **40**, e52-e52 (2012).
827 62. Waterhouse, A.M., Procter, J.B., Martin, D.M., Clamp, M. & Barton, G.J. Jalview Version 2--a multiple
828 sequence alignment editor and analysis workbench. *Bioinformatics* **25**, 1189-1191 (2009).
829 63. Tamura, K., Stecher, G. & Kumar, S. MEGA11: Molecular Evolutionary Genetics Analysis Version 11.
830 *Mol Biol Evol* **38**, 3022-3027 (2021).
831 64. Bailey, T.L., Johnson, J., Grant, C.E. & Noble, W.S. The MEME Suite. *Nucleic Acids Res* **43**, W39-49 (2015).
832 65. Bailey, T.L. & Grant, C.E. SEA: Simple Enrichment Analysis of motifs. *bioRxiv* (2021).
833 66. Love, M.I., Huber, W. & Anders, S. Moderated estimation of fold change and dispersion for RNA-seq
834 data with DESeq2. *Genome Biol* **15**, 550 (2014).
835 67. Al-Izki, S., *et al.* Practical guide to the induction of relapsing progressive experimental autoimmune
836 encephalomyelitis in the Biozzi ABH mouse. *Mult Scler Relat Disord* **1**, 29-38 (2012).
837 68. Baker, D. & Amor, S. Publication guidelines for refereeing and reporting on animal use in experimental
838 autoimmune encephalomyelitis. *J Neuroimmunol* **242**, 78-83 (2012).
839 69. Maggi, P., Sati, P. & Massacesi, L. Magnetic resonance imaging of experimental autoimmune
840 encephalomyelitis in the common marmoset. *J Neuroimmunol* **304**, 86-92 (2017).
841 70. Nardo, G., *et al.* Transcriptomic indices of fast and slow disease progression in two mouse models of
842 amyotrophic lateral sclerosis. *Brain : a journal of neurology* **136**, 3305-3332 (2013).
843 71. Nardo, G., *et al.* Immune response in peripheral axons delays disease progression in SOD1(G93A) mice.
844 *J Neuroinflammation* **13**, 261 (2016).
845 72. Hampton, D.W., *et al.* HspB5 Activates a Neuroprotective Glial Cell Response in Experimental
846 Tauopathy. *Frontiers in neuroscience* **14**, 574 (2020).
847 73. Hampton, D.W., *et al.* Cell-mediated neuroprotection in a mouse model of human tauopathy. *J Neurosci*
848 **30**, 9973-9983 (2010).
849 74. Torvell, M., *et al.* A single systemic inflammatory insult causes acute motor deficits and accelerates
850 disease progression in a mouse model of human tauopathy. *Alzheimers Dement (N Y)* **5**, 579-591
851 (2019).

- 852 75. Duan, L., *et al.* PDGFRbeta Cells Rapidly Relay Inflammatory Signal from the Circulatory System to
 853 Neurons via Chemokine CCL2. *Neuron* **100**, 183-200 e188 (2018).
 854 76. Stuart, T., *et al.* Comprehensive Integration of Single-Cell Data. *Cell* **177**, 1888-1902 e1821 (2019).
 855 77. Khozoi, C., *et al.* scFlow: A Scalable and Reproducible Analysis Pipeline for Single-Cell RNA
 856 Sequencing Data. (Authorea Preprints, 2021).
 857 78. Tsartsalis, S., *et al.* Single nuclear transcriptional signatures of dysfunctional brain vascular
 858 homeostasis in Alzheimer's disease. (2021).
 859

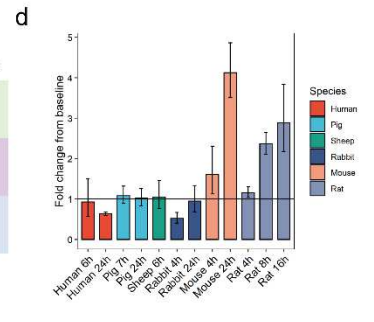
860 **Figures**



861 **Figure 1. *TSPO* gene expression and epigenetic profile in human and mouse**
 862 **macrophages. a,b** Forest plot of the meta-analysis for *TSPO* expression in **a** mouse and
 863 **b** human myeloid cells treated with a pro-inflammatory stimulus. The random-effect
 864 model was applied when combining the gene expression. The black squares represent the
 865 logFC value of each dataset. The horizontal lines indicate the 95% confidence intervals of
 866 each study. The diamond represents the pooled logFC. **c,d** ChIP-seq data, generated from
 867 mouse and **d** human myeloid cells treated with IFN γ , visualisation of histone
 868 modification peaks (H3K27Ac, H3K4me3, H3K4me1) and PU.1 binding peaks at *TSPO* loci
 869 in IFN γ -treated (pink) and baseline (blue) conditions. Yellow vertical shading
 870 corresponds to the TSS along with promoter and light blue shading corresponds to the
 871 enhancer region of the loci.
 872

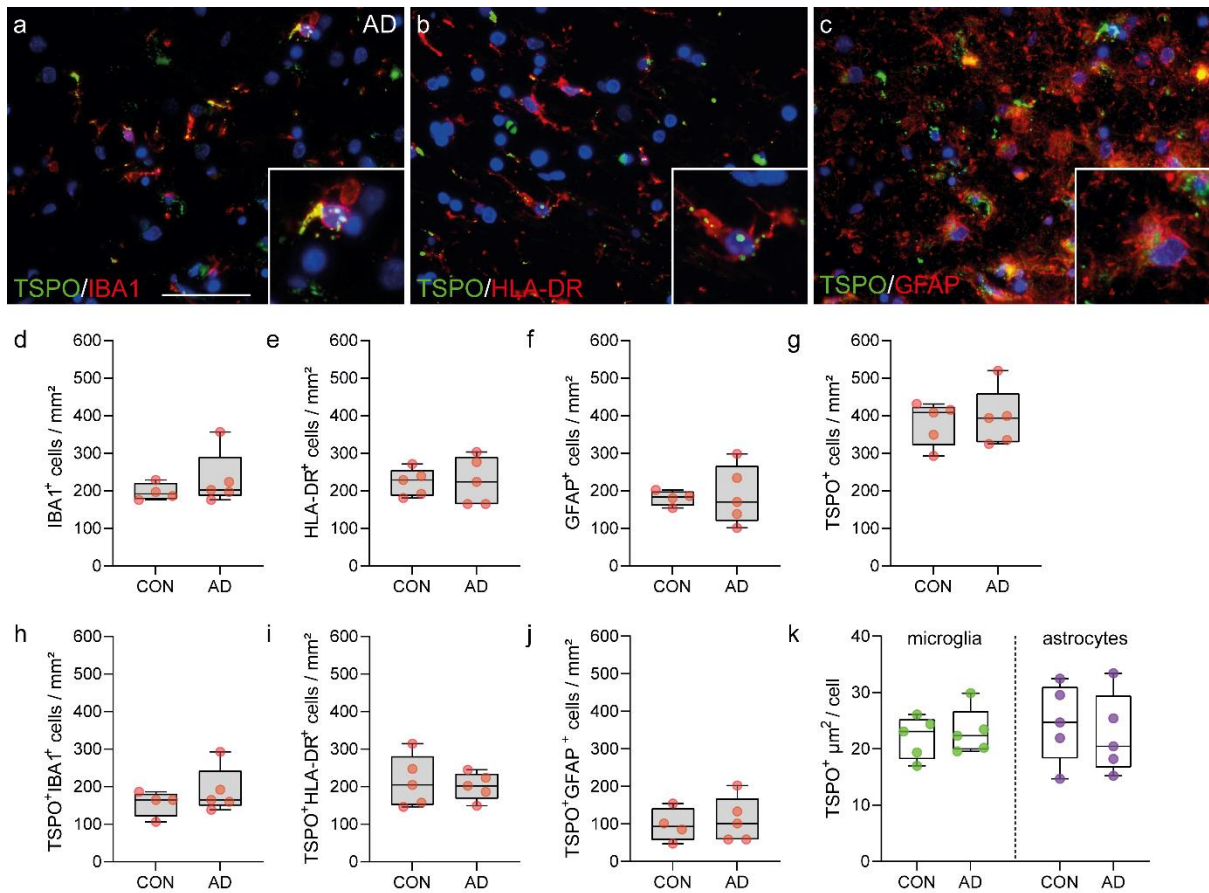


Motif ID	Motif Name	Consensus Motif	Enrichment Ratio	p-value	q-value
MA0099.2	AP1	TGACTCA	13	0	0.01
MA0080.1	ETS	VGGAS	6.5	0.2	0.3
MA0079.5	SP1	GGGGCGGGG	1.08	0.76	0.76



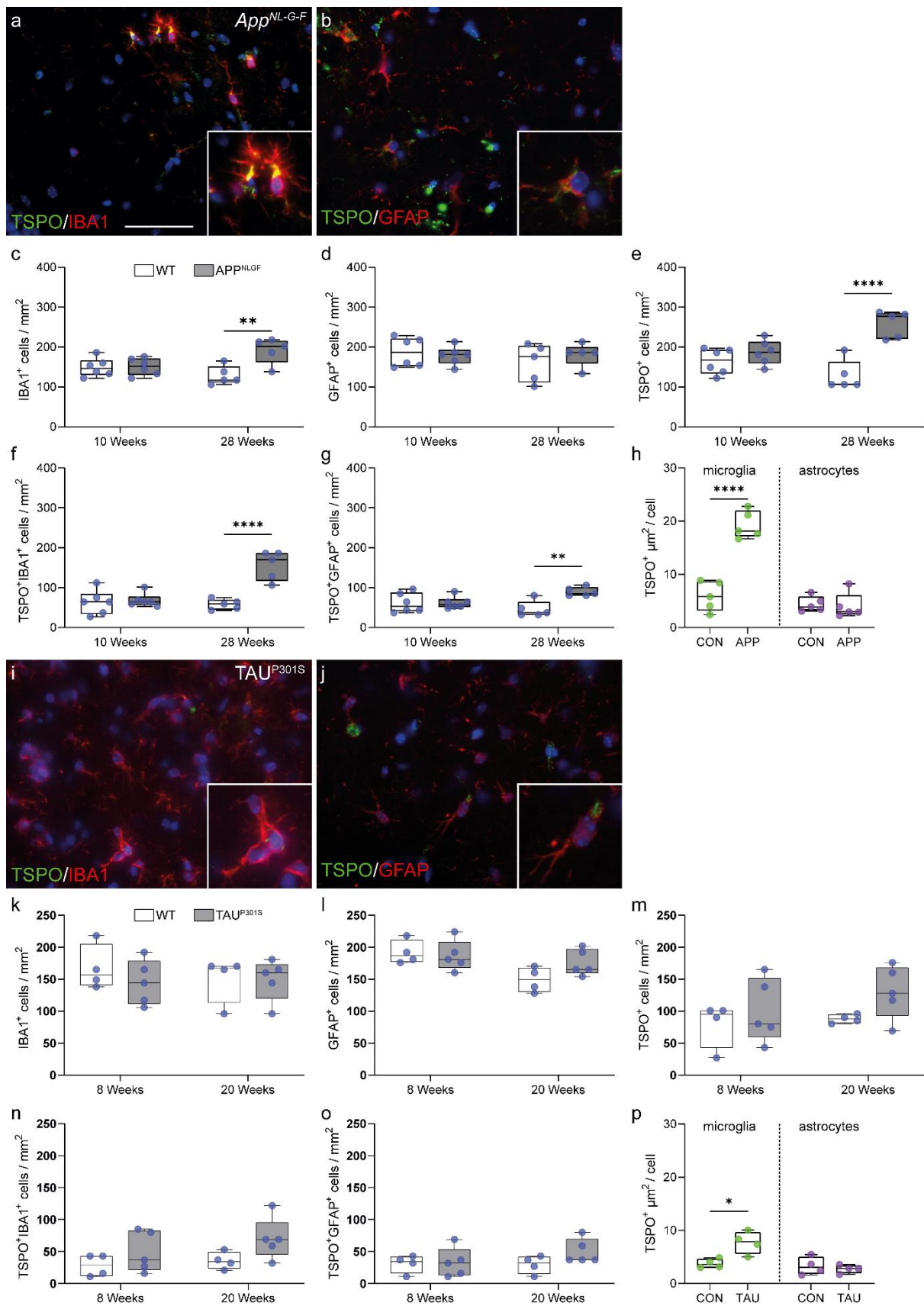
873

874 **Figure 2. AP1 binding site in the TSP0 promoter and LPS inducible TSP0 expression**
 875 **is unique to the Muroidea superfamily of rodents.** **a** Multiple sequence alignment of
 876 TSP0 promoter region of 15 species from primate, rodent, non-primate mammals. AP1
 877 (cyan) and an adjacent ETS (brown) site is present in only a sub-group of rodent family
 878 which includes mouse, rat and Chinese hamster. The ETS site which binds transcription
 879 factor PU.1 is present across species. SP1 (blue) site is found in the core promoter close
 880 to the TSS (green). For species where the TSS is not known Exon1 (pink) location is
 881 shown. Blue arrowhead indicates sequence without any motif hidden for visualization. **b**
 882 Phylogenetic tree is showing a clear branching of rat, mouse and Chinese hamster TSP0
 883 promoter from the rest of the species from rodents. Primates including marmoset forms
 884 a separate clade while sheep, cow and pig are part for the same branch. Green highlights
 885 represent species that contain the AP1 site in TSP0 promoter. Phylogenetic tree was
 886 generated using the Maximum Parsimony method in MEGA11. The most parsimonious
 887 tree with length = 4279 is shown. The consistency index (CI) is 0.760458 (0.697014) and
 888 the retention index is 0.656386 (RI) (0.656386) for all sites and parsimony-informative
 889 sites (in parentheses). The percentage of replicate trees in which the associated taxa
 890 clustered together in the bootstrap test (1000 replicates) are shown next to the branches.
 891 **c** TSP0 gene expression in macrophages or microglia isolated from multiple species after
 892 LPS stimulation. In line with the multiple sequence alignment of the TSP0 promoter,
 893 species (mouse, rat) that contains an adjacent AP1 and ETS motif shows an upregulation
 894 of TSP0 gene after LPS stimulation. Species lacking (human, pig, sheep, rabbit) those sites
 895 show a downregulation or no change in expression after stimulation. **d** Differential motif
 896 enrichment analysis between rodent vs non-rodent TSP0 promoter region by SEA tools
 897 from MEME-suite confirms the significant enrichment of AP1 site in rodent promoter
 898 whereas SP1 site does not show any differential enrichment. TSS; Transcription start site.



899

900 **Figure 3. TSPO expression is not altered in the AD hippocampus.** a-c Representative
 901 images of TSPO expression in microglia and astrocytes in AD hippocampus. d-g no
 902 increases were observed in microglia ($P=0.5159$, $U=7$, ranks=17, 28), activated microglia
 903 ($P=0.8997$, $t=0.1301$, $df=8$) astrocytes ($P = 0.8599$, $t=0.1831$, $df=7$) or TSPO+ cells ($P =$
 904 0.7329 , $t=0.3534$, $df=8$) in the AD hippocampus. h-j Concurrently no increases were
 905 observed in the number of TSPO+IBA1+ microglia ($P = 0.3573$, $t=0.9854$, $df=7$),
 906 TSPO+HLA-DR+ microglia ($P = 0.7239$, $t=0.3659$, $df=8$) and astrocytes ($P = 0.7181$,
 907 $t=0.3760$, $df=7$). k Even though microglia in the AD brain show signs of activation
 908 microglia do not upregulate TSPO expression in the hippocampus ($P = 0.6717$, $t=0.4398$,
 909 $df=8$), nor do astrocytes ($P = 0.6475$, $t=0.4750$, $df=8$). Statistical significance in d-k was
 910 determined by a two-tailed unpaired *t*-test or Mann-Whitney U-test when not normally
 911 distributed. Box and whiskers mark the 25th to 75th percentiles and min to max values,
 912 respectively, with the median indicated. Scale bar = 50µm, inserts are digitally zoomed in
 913 (200%).

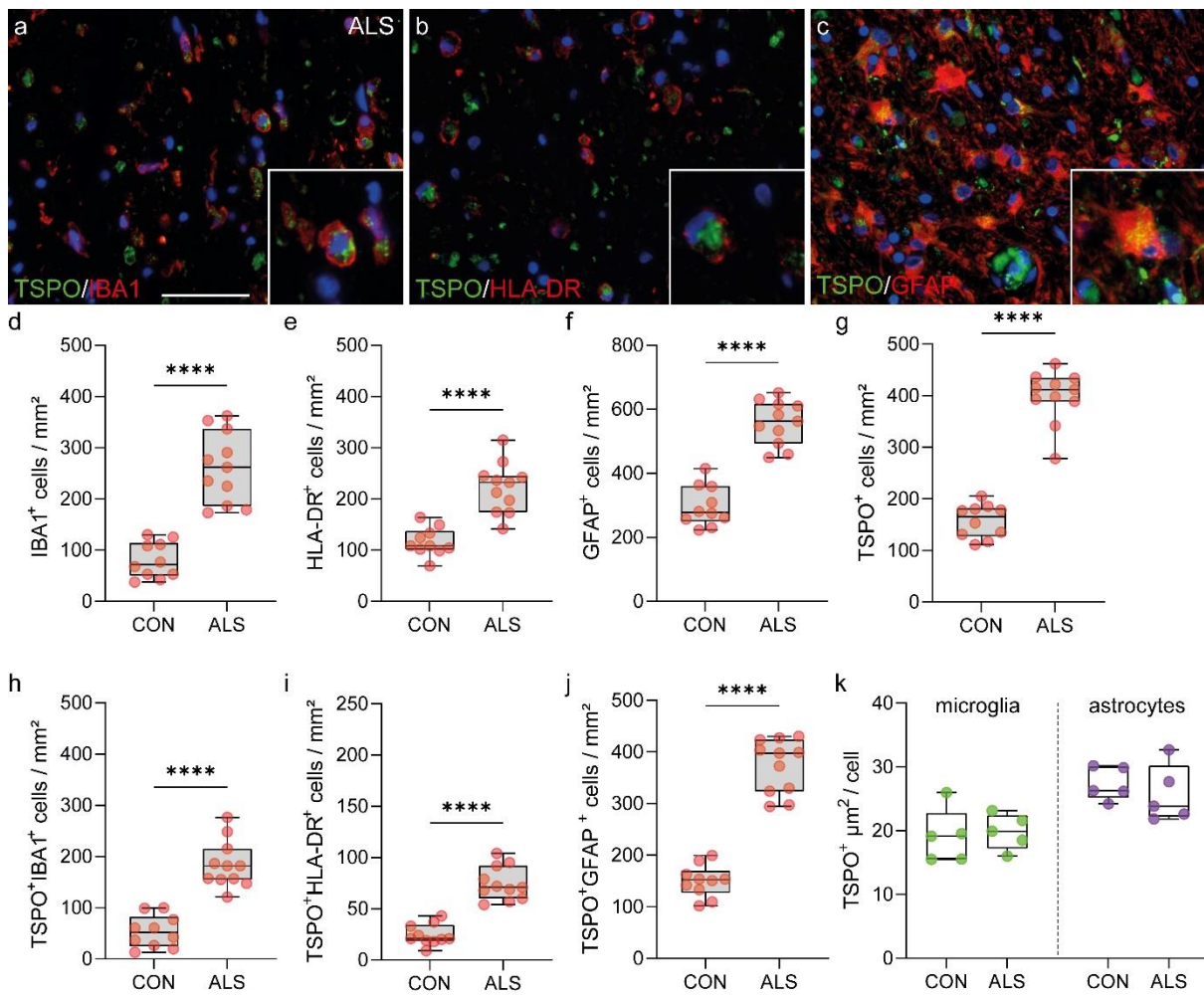


914

915 **Figure 4. Microglia in the *App^{NL-G-F}* and *TAU^{P301S}* model increase TSPO expression.**

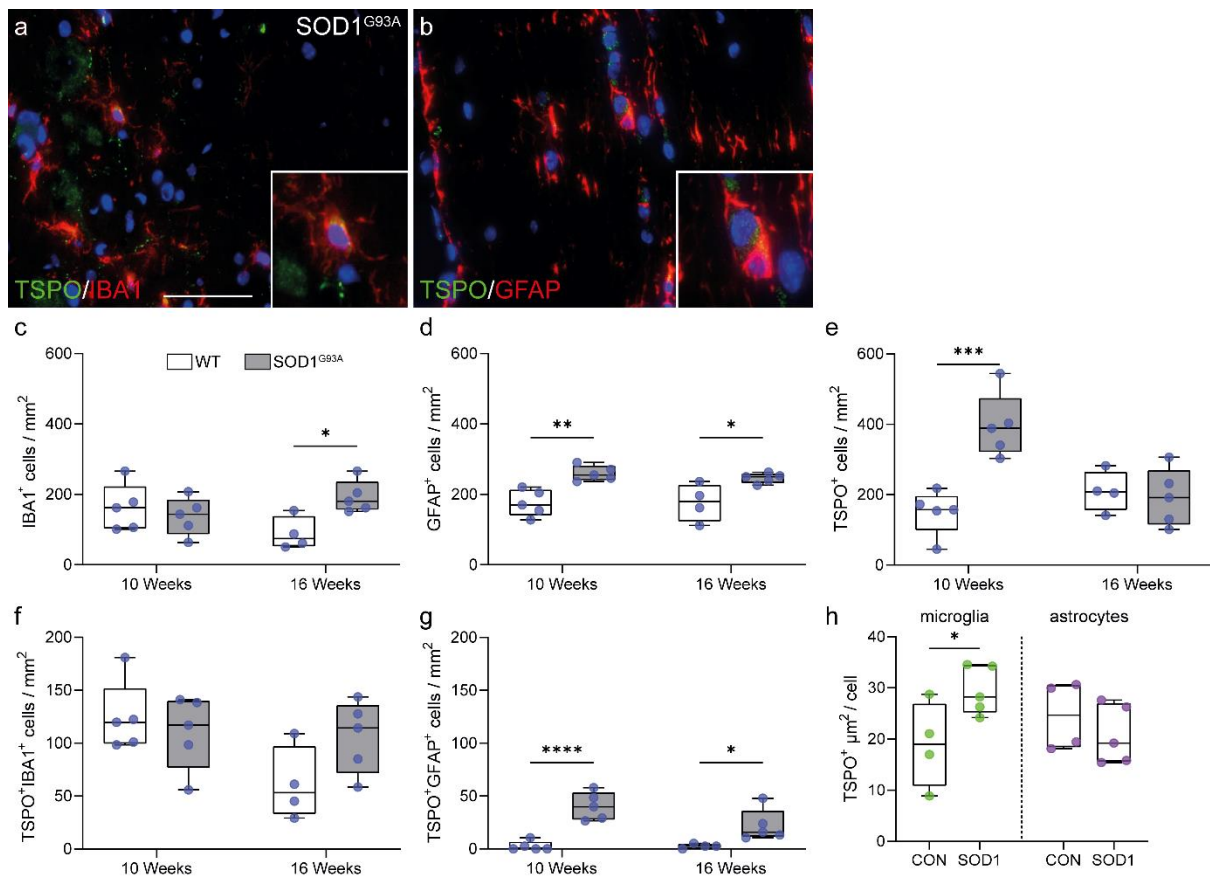
916 **a,b** Representative images of TSPO expression in microglia and astrocytes in *App^{NL-G-F}*

917 hippocampus. **c** An increase was observed in IBA1+ microglia at 28 weeks ($P = 0.0078$,
918 $t=3.522$, $df=8$) but not 10 weeks ($P = 0.8788$, $t=0.1565$, $df=10$) in *App^{NL-G-F}* hippocampus
919 compared to control. **d** No increase in astrocytes was observed (10 weeks: $P = 0.6266$,
920 $t=0.5019$, $df=10$; 28 weeks: $P = 0.4425$, $t=0.8080$, $df=8$). **e** TSPO+ cells were increased at
921 28 weeks ($P = 0.0079$, $U=0$, $ranks=15, 40$) but not at 10 weeks ($P = 0.2375$, $t=1.257$,
922 $df=10$) in the *App^{NL-G-F}* mice. **f,g** Both TSPO+ microglia ($P = 0.0005$, $t=5.658$, $df=8$) and
923 astrocytes ($P = 0.0030$, $t=4.207$, $df=8$) were increased at 28 weeks in the hippocampus of
924 *App^{NL-G-F}* mice but not at 10 weeks (microglia: $P = 0.7213$, $t=0.3670$, $df=10$; astrocytes: P
925 $= 0.9561$, $t=0.056$, $df=10$). **h** Activated microglia ($P < 0.0001$, $t=7.925$, $df=8$), but not
926 astrocytes ($P = 0.3095$, $U=7$, $ranks=33, 22$), in the *App^{NL-G-F}* model have increased TSPO
927 expression. **i,j** Representative images of TSPO expression in microglia and astrocytes in
928 *TAUP^{301S}* hippocampus. **k-m** No increases in microglia (8 weeks: $P = 0.3687$, $t=0.9608$,
929 $df=7$; 20 weeks; $P = 0.9647$, $t=0.04580$, $df=7$), astrocytes (8 weeks: $P = 0.7353$, $t=0.3519$,
930 $df=7$; 20 weeks; $P = 0.0870$, $t=1.989$, $df=7$) or TSPO+ cells (8 weeks: $P = 0.8492$, $U=9$,
931 $ranks=19, 26$; 20 weeks; $P = 0.0876$, $t=1.985$, $df=7$) were observed in the hippocampus of
932 *TAUP^{301S}* mice. **n,o** No increase was observed in the number of TSPO+ microglia (8 weeks:
933 $P = 0.2787$, $t=1.174$, $df=7$; 20 weeks; $P = 0.0907$, $t=1.961$, $df=7$) or astrocytes (8 weeks: P
934 $= 0.8684$, $t=0.1718$, $df=7$; 20 weeks; $P = 0.1984$, $U=4.5$, $ranks=14.5, 30.5$). **p** Microglia in
935 the *TAUP^{301S}* increase TSPO expression ($P = 0.0133$, $t=3.471$, $df=6$) whereas astrocytes do
936 not ($P = 0.5800$, $t=0.5849$, $df=6$). Statistical significance in **c-h** and **k-p** was determined
937 by a two-tailed unpaired *t*-test or Mann-Whitney U-test when not normally distributed.
938 Box and whiskers mark the 25th to 75th percentiles and min to max values, respectively,
939 with the median indicated. Scale bar = 50 μ m, inserts are digitally zoomed in (200%).



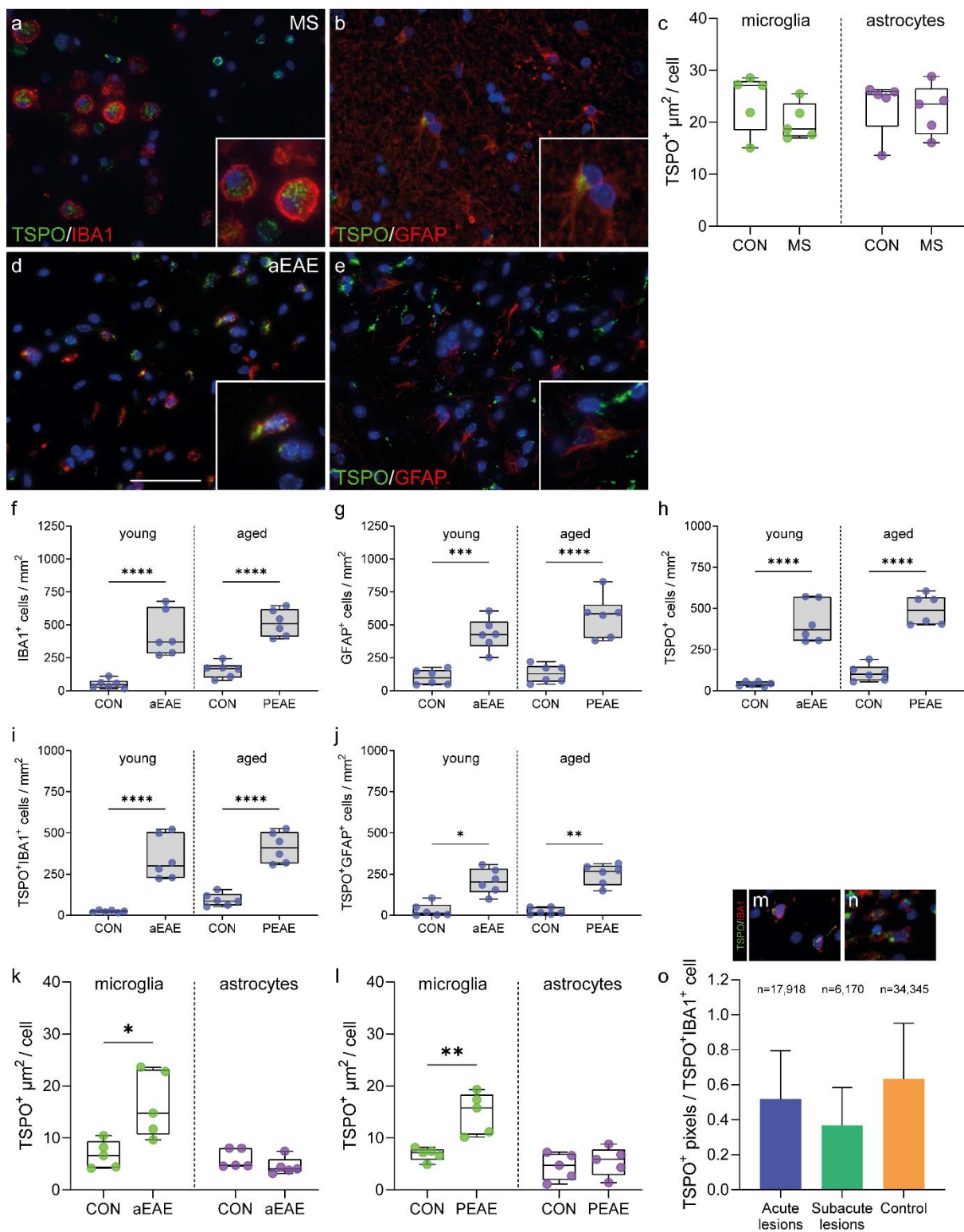
940

941 **Figure 5. TSP0 is expressed by microglia and astrocytes but not increased in ALS**
 942 **spinal cord. a-c** Representative images of TSP0 expression in microglia and astrocytes
 943 in ALS spinal cord. **d-f** An increase was observed in microglia ($P < 0.0001$, $t=7.445$, $df=19$),
 944 HLA-DR+ microglia ($P < 0.0001$, $t=6.007$, $df=19$), and astrocytes ($P < 0.0001$, $t=9.024$,
 945 $df=19$) in ALS spinal cord when compared to controls. **g** A 2.5-fold increase of TSP0+ cells
 946 ($P < 0.0001$, $t=12.88$, $df=19$) was observed in the ALS spinal cord. **h,i** Up to a 3.4-fold
 947 increase in the density of TSP0+ microglia (TSP0+IBA1+ cell, $P < 0.0001$, $t=7.541$, $df=19$)
 948 (TSP0+HLA-DR+ cells, $P < 0.0001$, $t=3.368$, $df=19$) was observed. **j** TSP0+ astrocytes
 949 were significantly increased ($P < 0.0001$, $t=11.77$, $df=19$) in the spinal cord of ALS
 950 patients. **k** The increase in activated microglia and astrocytes was not associated with an
 951 increase in TSP0 expression in microglia ($P = 0.7684$, $t=0.3046$, $df=8$) or in astrocytes (P
 952 $= 0.5047$, $t=0.6985$, $df=8$). Statistical significance in **d-k** was determined by a two-tailed
 953 unpaired t -test. Box and whiskers mark the 25th to 75th percentiles and min to max values,
 954 respectively, with the median indicated. Scale bar = 50 μ m, inserts are digitally zoomed in
 955 (200%).



956

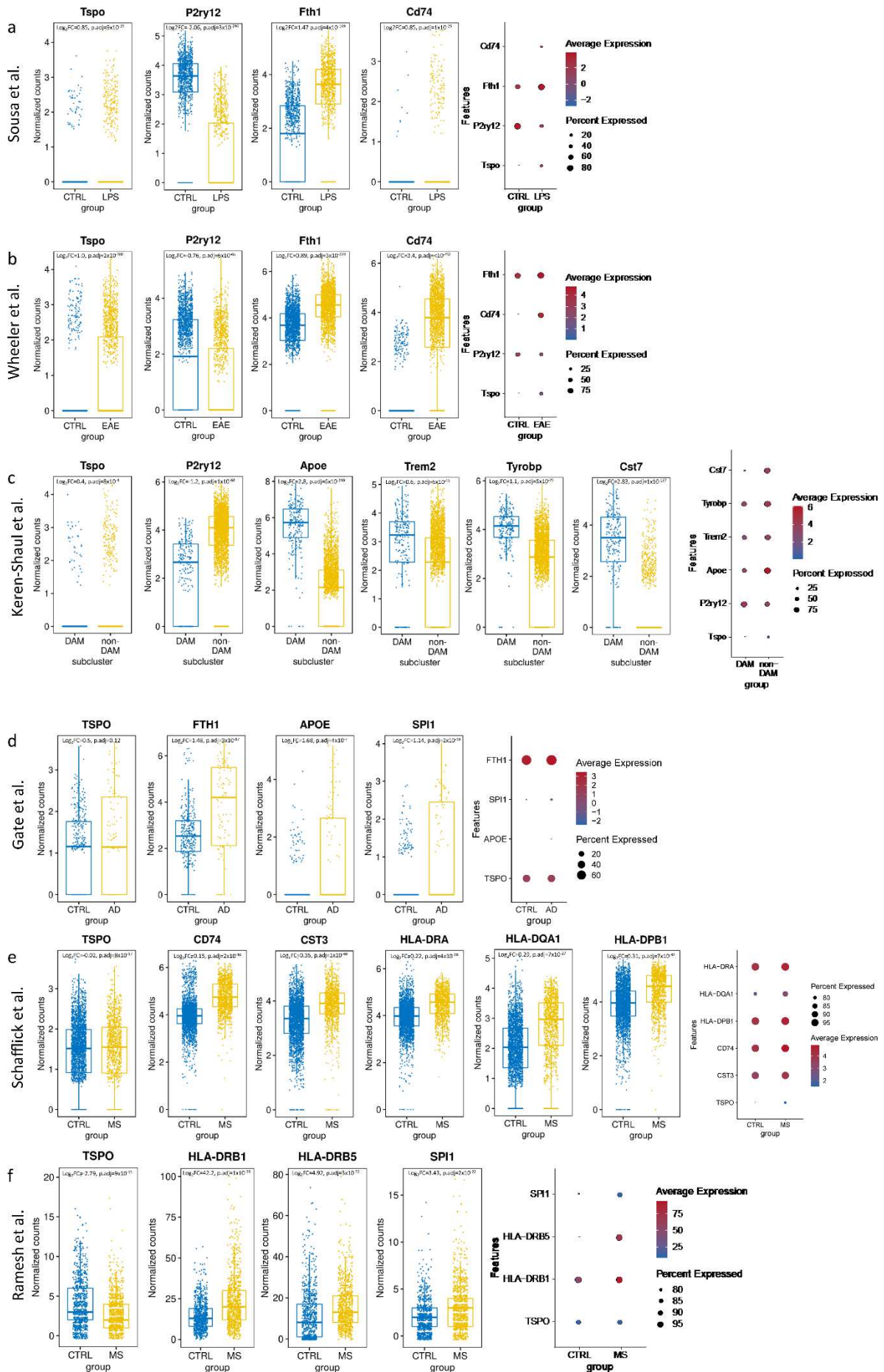
957 **Figure 6. Microglia in the SOD1^{G93A} model increase TSPO expression.** **a,b**
 958 Representative images of TSPO expression in microglia and astrocytes in SOD1^{G93A} spinal
 959 cord. **c** An increase was observed in microglia in SOD1^{G93A} spinal cord when compared to
 960 controls at 16 weeks ($P=0.0115$, $t=3.395$, $df=7$) but not at 10 weeks ($P = 0.5334$, $t=0.6509$,
 961 $df=8$). **d** An increase for astrocytes was observed for both 10 weeks ($P = 0.0024$, $t=4.362$,
 962 $df=8$) and 16 weeks ($P = 0.0248$, $t=2.848$, $df=7$) **e** An increase in TSPO+ cells was observed
 963 at 10 weeks ($P = 0.0011$, $t=4.931$, $df=8$) but not 16 weeks ($P = 0.7299$, $t=0.3594$, $df=7$). **f**
 964 No increase in the number of TSPO+ microglia was observed (10 weeks: $P = 0.5244$,
 965 $t=0.6656$, $df=8$; 16 weeks, $P = 0.0930$, $t=1.944$, $df=7$). **g** TSPO+ astrocytes were increased
 966 up to 15-fold in the spinal cord of SOD1^{G93A} mice (10 weeks: $P = 0.0003$, $t=6.085$, $df=8$; 16
 967 weeks: $P = 0.382$, $t=2.548$, $df=7$). **h** Despite no increase in the number of TSPO+ microglia,
 968 an increase in the amount of TSPO per cell was observed in microglia ($P = 0.0451$, $t=2.435$,
 969 $df=7$), but not astrocytes ($P = 0.4052$, $t=0.8856$, $df=7$). Statistical significance in **c-h** was
 970 determined by a two-tailed unpaired *t*-test. Box and whiskers mark the 25th to 75th
 971 percentiles and min to max values, respectively, with the median indicated. Scale bar =
 972 50 μ m, inserts are digitally zoomed in (200%).



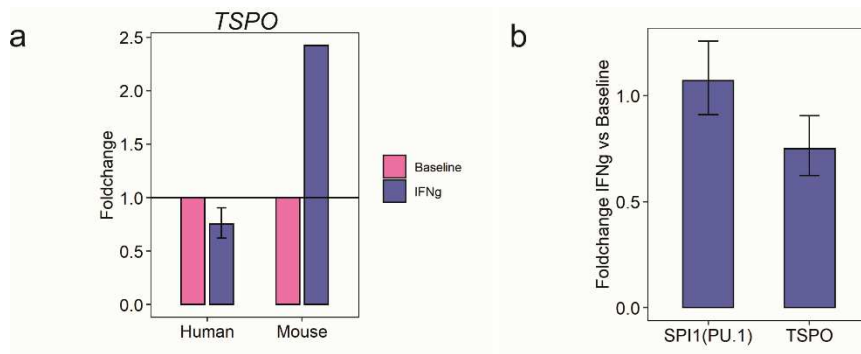
973

974 **Figure 7. Microglia in mouse aEAE and PEAE, and marmoset EAE, but not MS,**
 975 **increase TSPO expression. a,b** Representative images of TSPO+ microglia and
 976 astrocytes in MS. **c** TSPO+ microglia ($P = 0.2278$, $t=1.306$, $df=8$) and astrocytes ($P =$
 977 0.5476 , $U=9$, $\text{ranks}=31, 24$) do not increase TSPO expression in MS. **d,e** Representative
 978 images of TSPO expression in microglia and astrocytes in EAE mice. **f-h** microglia ($P <$
 979 0.0001 , $F_{(3,20)}=25.68$), astrocyte ($P < 0.0001$, $F_{(3,20)}=25.51$), and TSPO+ cell numbers ($P <$

980 0.0001, $F_{(3,20)}=44.53$), are increased during disease in aEAE mice and PEAE. **i,j** An
981 increase in both TSPO+ microglia ($P < 0.0001$, $F_{(3,20)}=30.93$) and TSPO+ astrocytes ($P =$
982 0.0005 , $K-W=17.72$) is observed during disease. **k,l** TSPO+ microglia increase TSPO
983 expression in aEAE mice ($P = 0.0136$, $t=3.152$, $df=8$), and in PEAE mice ($P = 0.0028$,
984 $t=4.248$, $df=8$). Astrocytes do not increase TSPO expression in aEAE ($P = 0.0556$, $U=3$,
985 $ranks=37, 18$), and PEAE ($P = 0.5918$, $t=0.5584$, $df=8$). **m,n** Representative images of
986 TSPO+ microglia in marmoset EAE. **o** TSPO+ pixels are not increased in acute and
987 subacute lesions in marmoset EAE relative to control. Statistical significance in **f-j,o** was
988 determined by a one way ANOVA or Kruskal-Wallis test when not normally distributed,
989 and by a two-tailed unpaired t -test or Mann-Whitney U-test when not normally
990 distributed in **c,k** and **l**. Holm-Sidak's and Dunn's multiple comparisons were performed.
991 Box and whiskers mark the 25th to 75th percentiles and min to max values, respectively,
992 with the median indicated. Scale bar = 50 μ m, inserts are digitally zoomed in (200%).

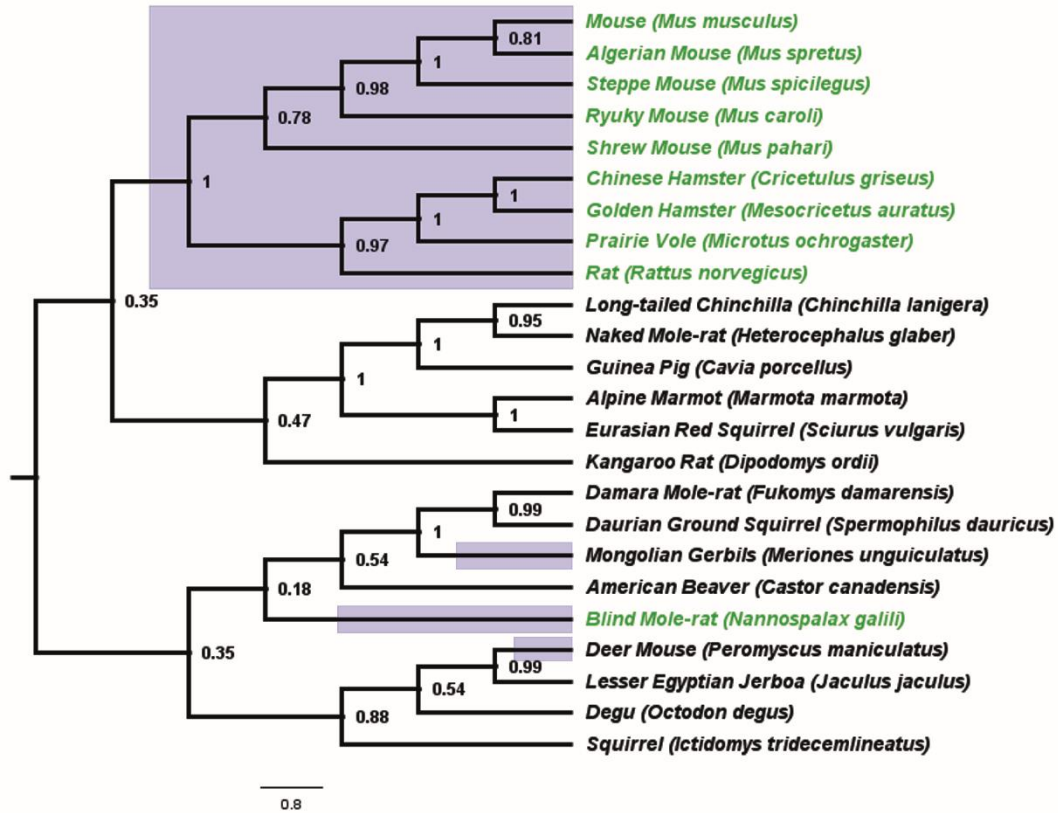


994 **Figure 8. TSPO is increased in mouse but not human pro-inflammatory activated**
995 **and disease-associated microglia. a-c** Boxplots and dotplots showing the significantly
996 elevated expression of *Tspo* in mouse models of pro-inflammatory activation using LPS
997 (GSE115571), of acute EAE (GSE130119) and of AD (GSE98969). The percentage of cells
998 that express *Tspo* in mouse microglia is relatively low, but it is considerably increased
999 after LPS treatment, in the EAE model and in the DAM cells. **d-f** TSPO is not significantly
1000 upregulated in microglia-like cells from the CSF of AD (GSE134578) and MS (GSE138266)
1001 patients. The percentage of cells that express a given gene corresponds to the size of the
1002 dot, whereas the average expression corresponds to the fill colour of the dot.



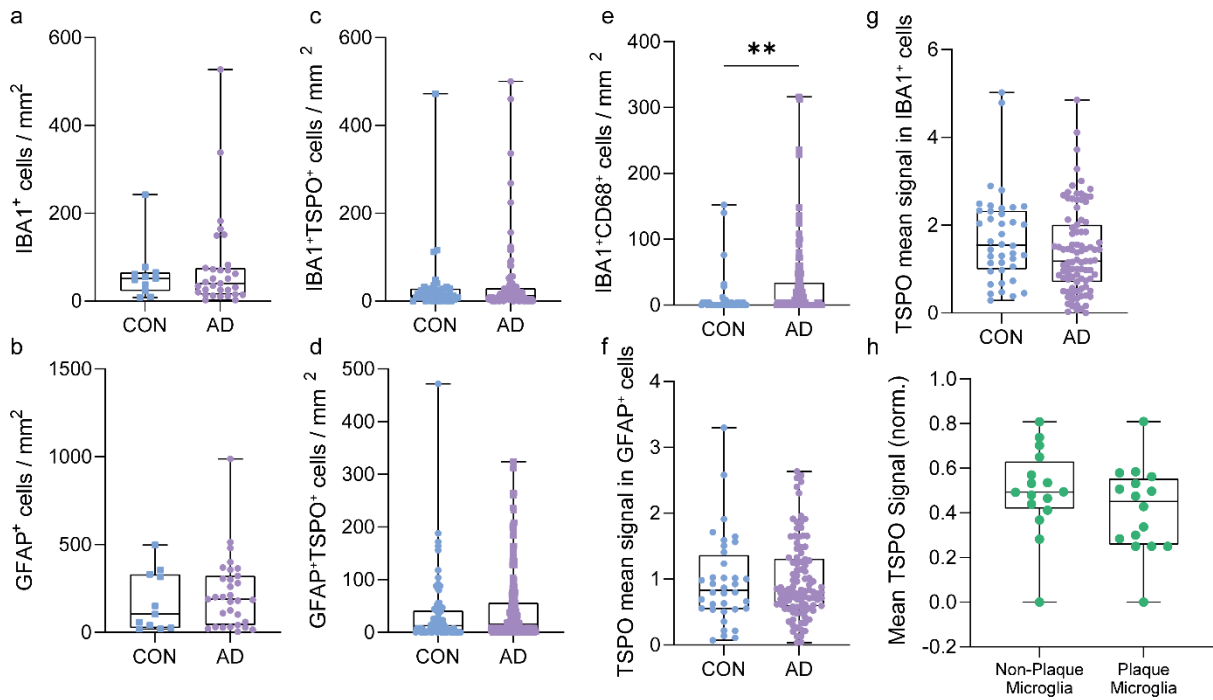
1003

1004 **Figure S1. a** Barplot showing TSPO fold change in human and mouse macrophages in
 1005 baseline and IFN γ treated samples. **b** Barplot showing PU.1 (SPI1) transcription factor
 1006 and TSPO gene expression change in IFN γ treated macrophage compared to baseline
 1007 condition.



1008

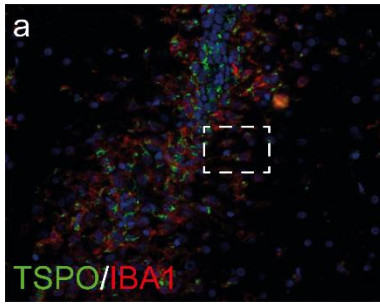
1009 **Figure S2.** Of the 24 rodent species examined here, 12/24 are from the Muroidea
 1010 superfamily (purple branches). 10 of these 12 Muroidea species contain the AP1 binding
 1011 site in the TSPO promoter (Green Highlight). We did not find any rodent species outside
 1012 the Muroidea superfamily that contain the AP1 binding site in the TSPO promoter. The
 1013 phylogenetic analysis shows that majority of the species (9/12) from Muroidea
 1014 superfamily forms a single clade. Phylogenetic tree was generated using the Maximum
 1015 Parsimony method in MEGA11. The CI is 0.623399 (0.553120) and the RI is 0.525671
 1016 (0.525671) for all sites and parsimony-informative sites (in parentheses). The
 1017 percentage of replicate trees in which the associated taxa clustered together in the
 1018 bootstrap test (1000 replicates) are shown next to the branches.



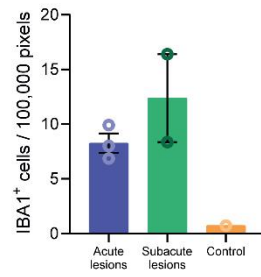
1019

1020 **Figure S3. a-d** no increase in total or TSPO+ microglia (P) and astrocytes (P) are observed
 1021 in control versus AD. **e** An increase in CD68+IBA1+ cells is observed in AD. **f,g** No
 1022 increases in mean TSPO signal in microglia and astrocytes is observed in AD relative to
 1023 control. **h** No differences are observed in mean TSPO signal in microglia associated with
 1024 plaques compared to mean TSPO signal in microglia that are distant from plaques.

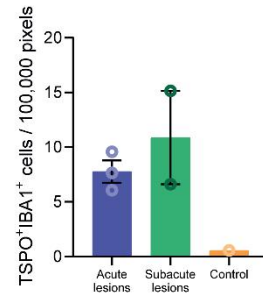
1025



b



c



1026

1027

1028

Figure S4. a Representative image of an acute lesion in marmoset EAE. IBA1+ and TSPO+IBA1+ cells are increased in acute and subacute lesions compared to white matter in control marmoset.

1029 Supplementary Table 1. Clinical details of AD and control cases

Case	Age/sex	Diagnosis	Region	Braak stage	PMD, h:min
AD cases					
1	81/F	AD	HC (anterior)	6	05:30
2	88/F	AD	HC (anterior)	6	06:19
3	62/M	AD	HC (anterior)	6	06:15
4	64/F	AD	HC (anterior)	6	06:30
5	76/M	AD	HC (anterior)	6	04:40
Controls					
1	65/F	NDC	HC	2	07:10
2	90/F	NDC	HC	3	06:10
3	81/F	NDC	HC	3	05:30
4	77/M	NDC	HC (anterior)	2	04:30
5	81/F	Ischemic changes	HC (anterior)	4	05:50

1030 Abbreviations: F – female; HC – hippocampus; M – male; NDC – non-demented control; PMD – postmortem delay.

1031 Supplementary Table 2. Clinical details of ALS and control cases

Case	Age/ sex	Diagnosis	DD, months	Cause of death	PMD, h	Primary onset	SPC levels
ALS short disease duration							
1	70/F	sALS	6	respiratory failure	< 12	leg	C/T/L
2	63/M	sALS	7	respiratory failure	< 12	leg	C/T/L
3	61/F	sALS	12	euthanasia	< 12	arm	C/T/L
4	60/M	sALS	12	euthanasia	< 12	arm	C/T/L
5	81/M	sALS	12	respiratory failure	< 12	respiratory	T/L
6	84/F	sALS	13	euthanasia	< 12	bulbar	C/T
7	56/F	sALS	16	euthanasia	< 12	leg	C/T/L
ALS medium disease duration							
8	43/M	sALS	36	unknown	< 12	arm	C/T/L
9	64/F	fALS	57	pneumonia	< 12	leg	C/T/L
10	68/M	sALS	87	euthanasia	< 12	arm	C/T/L
11	79/M	sALS (C9orf72)	107	pneumonia	< 12	arm	C/T/L
Controls							
12	60/M	bricker-bladder	N/A	lung embolism	< 24	N/A	C/T/L
13	63/M	kidney carcinoma	N/A	lung embolism	< 24	N/A	C/T/L
14	81/F	heart ischemia	N/A	endocarditis	< 24	N/A	C/T/L
15	63/F	adeno-carcinoma	N/A	paralytic ileus	< 24	N/A	C/T/L
16	69/M	oesophagus carcinoma	N/A	multi-organ failure	< 24	N/A	C/T/L
17	78/F	cholangio-carcinoma	N/A	multi-organ failure	< 24	N/A	T
18	75/M	COPD, pneumonia	N/A	respiratory failure	< 12	N/A	C/T
19	59/F	pleuritis carcinomatosa	N/A	respiratory failure	< 24	N/A	C/T/L
20	47/F	pancreas carcinoma	N/A	abdominal bleeding	< 24	N/A	C/T/L
21	54/F	gallbladder carcinoma	N/A	heart failure	< 48	N/A	C/T/L

1032 1033 Abbreviations: C – cervical; COPD – chronic obstructive pulmonary disease; DD – disease duration; F – female; fALS – familial ALS; L – lumbar; M – male; PMD – postmortem delay; S – sacral; sALS – sporadic ALS; SPC – spinal cord; T – thoracic.

1034 Supplementary Table 3. Clinical details of MS and control cases

Case	Age/sex	Diagnosis	Disease duration, years	Cause of death	PMD, h:min
MS cases					
1	35/F	SPMS	10	Euthanasia	10:20
2	54/F	SPMS	27	Respiratory failure	9:25
3	50/F	SPMS	18	Euthanasia	9:05
4	50/M	SPMS	21	Unknown	10:50
5	63/F	Unknown	Unknown	Unknown	10:50
Controls					
1	84/M	NNC	N/A	Heart failure	5:35
2	89/F	NNC	N/A	Pneumonia	3:52
3	79/M	NNC	N/A	Heart failure	6:20
4	73/F	NNC	N/A	Mamma carcinoma	7:45
5	87/F	NNC	N/A	Pneumonia	7:00

1035 Abbreviations: F - female; M - male; N/A - not applicable; NNC - non-neurological control; PMD - postmortem delay; SPMS -
 1036 secondary progressive multiple sclerosis.

1037 Supplementary Table 4. Clinical History of mice with EAE

Mouse number	Sampling day	Age (weeks)
Acute young (aEAE)		
1	14 (4)	10-15
2	12 (4)	10-15
3	15 (4.5)	10-15
4	15 (4)	10-15
5	13 (4.5)	10-15
6	20 (4.5)	10-15
Acute old (PEAE)		
1	15 (4.5)	> 50
2	13 (5)	> 50
3	13 (4.5)	> 50
4	16 (4.5)	> 50
5	15 (5)	> 50
6	17 (4.5)	> 50

1038 EAE mice were immunized with SCH in CFA and monitored (sampling day refers to the day after immunization). Indicated clinical
 1039 scores are the maximal scores during neurological episodes of EAE. Abbreviations: EAE - experimental autoimmune
 1040 encephalomyelitis; aEAE - acute EAE, PEAE - **progressive EAE** .

1041 Supplementary Table 5. Clinical History of Marmosets

Animal ID	Gender	Disease Status	Age at EAE induction (years)	Disease duration (days)	Age (years)
1	M	Control	N/A	N/A	3
4	F	EAE	2.0	32	2.1
5	F	EAE	1.6	105	1.9
8	F	EAE	1.6	123	1.9

1042 Abbreviations: EAE - experimental autoimmune encephalitis; N/A - not applicable.

1043 Supplementary Table 6. Antibodies for immunohistochemistry and imaging mass
 1044 cytometry

Antigen	Species (isotype)	Clonality	Dilution	Antigen Retrieval	Product Number	Supplier
TSPO	goat	pAb	1:750	Citrate	NB100-41398	Novus Biologicals
TSPO	rabbit	mAb	1:750	Citrate	AB109497	Abcam
IBA1	rabbit	pAb	1:10000	Tris-EDTA	019-19741	Wako
IBA1	goat	pAb	1:1000	Tris-EDTA	AB48004	Abcam
IBA1	guinea pig	pAb	1:100	Citrate	234004	Synaptic Systems
GFAP	chicken	pAb	1:500	Citrate	AB5541	Millipore
HLA-DR	mouse (IgG2B)	mAb	1:750	Citrate	14-9956-82	Invitrogen
A β IC16	mouse (IgG2A)	mAb	1:400	Citrate	N/A	in-house ^a
P-Tau AT8	mouse (IgG1)	mAb	1:400	Citrate	AB_223647	Invitrogen
PLP	mouse (IgG2A)	mAb	1:200	Citrate	MCA839G	Bio-Rad
IMC	Ln-Isotope					
CD68	159Tb		1:800	EDTA	3159035D	Fluidigm
GFAP	162Dy		1:600	EDTA	Ab218309	Abcam
HLA-DR	174Yb		1:400	EDTA	3174025D	Fluidigm
IBA1	169Tm		1:3000	EDTA	019-197471	Wako
TSPO	149Sm		1:400	EDTA	Ab213654	Abcam

1045 ^aWith permission from Carsten Korth, Heinrich Heine University, Düsseldorf, Germany. Abbreviations: GFAP – glial fibrillary acidic
 1046 protein; IBA1 – ionized calcium-binding adaptor molecule 1; mAb – monoclonal antibody; pAb – polyclonal antibody; P-Tau –
 1047 phosphorylated Tau (Ser202, Thr205).

Supplementary Files

This is a list of supplementary files associated with this preprint. Click to download.

- [StatisticalanalysesFinal.docx](#)